Review

A topic review on probing primordial black hole dark matter with scalar induced gravitational waves

Chen Yuan[1,2,*] and Qing-Guo Huang[1,2,3,4,*]

SUMMARY

Primordial black holes (PBHs) might form from the collapse of over-densed regions generated by large scalar curvature perturbations in the radiation dominated era. Despite decades of various independent observations, the nature of dark matter (DM) remains highly puzzling. Recently, PBH DM have aroused interest since they provide an attracting explanation to the merger events of binary black holes discovered by LIGO/VIRGO and may play an important role on DM. During the formation of PBH, gravitational waves will be sourced by linear scalar perturbations at second-order, known as the scalar induced gravitational waves (SIGWs), which provides a new way to hunt for PBH DM. This topic review mainly focuses on the physics about SIGWs accompanying the formation of PBH DM.

INTRODUCTION

Primordial black holes (PBHs) have aroused interest recently, not only because they can represent the dark matter (DM) in our Universe but also can explain the binary black hole mergers events Sasaki et al. (2016); Chen and Huang (2018); Raidal et al. (2019); De Luca et al. (2020a); Hall et al. (2020); Bhagwat et al. (2021); Hütsi et al. (2020) discovered by LIGO Abbott et al., (2016) if $\sim 10^{-3}$ DM is in the form of PBHs. So far, there is no evidence for PBHs. Although various observations have constrained the fraction of DM in the form of PBHs Tisserand et al., (2007); Carr et al. (2010); Barnacka et al. (2012); Griest et al. (2013); Graham et al. (2015); Brandt (2016); Chen et al. (2016); Wang et al. (2018); Gaggero et al. (2017); Ali-Haimoud and Kamionkowski (2017); Aloni et al. (2017); Horowitz (2016); Niikura et al. (2019a); Zumalacarregui and Seljak (2018); Nakama et al. (2018); Abbott et al., (2018); Magee et al. (2018); Chen et al. (2019a); Niikura et al. (2019b); Chen and Huang (2019); Abbott et al. (2019); Wang et al. (2019a), f_{pbh}, there still exist an open window in the mass range of $[10^{-16}, 10^{-14}] \cup [10^{-13}, 10^{-12}] M_\odot$, where PBHs are possible to present all the DM in our Universe.

PBH is an old conception and it can date back to 1974 when Hawking and Carr proposed that black holes can be generated due to the collapse of over-densed regions in the early universe Carr and Hawking (1974); Carr (1975). The formation of PBHs is a threshold process. Once scalar perturbations exceed a critical value, they would generate an over-densed region which would immediately undergo gravitational collapse to form a single PBH when the comoving size of such region is of the order of the horizon size. The exact calculation of the PBH mass function, β, which describes the mass fraction of the Universe contained within PBHs at the formation time is still a debating and complicated question by today.

Among all the constraints on PBH DM, the scalar induced gravitational waves (SIGWs) provide a quite stringent constraint which can be several orders of magnitude better than the other constraints Chen et al. (2019b) in a certain mass range of PBHs. During radiation dominant (RD) epoch, scalar perturbations will alter the quadrupolar moment of the radiation and thus emit GWs at second-order Tomita (1967); Matarrese et al. (1993, 1994, 1998); Noh and Hwang (2004); Carbone and Matarrese (2005); Nakamura (2007). Therefore, SIGWs were inevitably generated during the formation of PBHs, providing a powerful tool to hunt for PBH DM. Moreover, PBHs are generated by large perturbations at small scales much larger than those on CMB scales; the second-order GWs induced by the enhanced perturbations sourced by the linear perturbations may exceed the first-order tensor inflationary modes Saito and Yokoyama (2009). See more relevant studies for SIGWs in Ananda et al. (2007); Baumann et al. (2007); Saito and Yokoyama (2009); Arroja et al. (2009); Assadullahi and Wands (2010); Bugaev and Klimai (2010a, b); Saito and Yokoyama (2010); Bugaev and Klimai (2011); Alabidi et al. (2013); Nakama and Suyama (2016); Nakama et al. (2017); Inomata et al. (2017a); Orlofsky

[1]School of Physical Sciences, University of Chinese Academy of Sciences, No. 19A Yuquan Road, Beijing 100049, China

[2]CAS Key Laboratory of Theoretical Physics, Institute of Theoretical Physics, Chinese Academy of Sciences, Beijing 100190, China

[3]Center for Gravitation and Cosmology, College of Physical Science and Technology, Yangzhou University, Yangzhou 225009, China

[4]School of Fundamental Physics and Mathematical Sciences Hangzhou Institute for Advanced Study, UCAS, Hangzhou 310024, China

*Correspondence:
yuanchen@itp.ac.cn (C.Y.),
huangqg@itp.ac.cn (Q.-G.H.)
https://doi.org/10.1016/j.isci.2021.102860

et al. (2017); Garcia-Bellido et al. (2017); Sasaki et al. (2018); Espinosa et al. (2018); Kohri and Terada (2018a); Cai et al. (2019a); Bartolo et al. (2019a, b); Unal (2019); Byrnes et al. (2019); Inomata and Nakama (2019); Clesse et al. (2018); Cai et al. (2019b); Inomata et al. (2019a, b); Cai et al. (2019c); Yuan et al. (2019a); Cai et al. (2019d); Lu et al. (2019); Yuan et al. (2019b); Tomikawa and Kobayashi (2019); De Luca et al. (2019a); Yuan et al. (2019c); Inomata et al. (2020a, b, c); Yuan and Huang (2020); Papanikolaou et al. (2020); Zhang et al. (2020a); Kapadia et al. (2020a); Zhang et al. (2020b); Domènech et al. (2020a); Dalianis and Kouvaris (2020); Atal and Domènech (2021). The SIGWs from PBHs are first calculated by Saito and Yokoyama in Saito and Yokoyama (2009), where they evaluate the energy density of SIGWs from monochromatic PBHs. They found that SIGWs from the current PBH DM in our Universe could be detected by pulsar timing arrays (PTAs) and space-based GW detectors. After the detection of GWs, intriguing studies emerged in this field in the recent years and there are hundreds of studies concerning SIGWs from PBHs so far.

Since there are a lot of reviews on PBHs in literature, e.g. some recent reviews given in Carr et al. (2020); Green and Kavanagh (2020); Carr and Kuhnel (2020), we mainly focus on SIGWs inevitably generated during the formation of PBHs in this paper. This paper will be organized as follows. In the section of Formation of PBHs, we give a brief introduction to the formation of PBHs. The physics about the SIGWs will be reviewed in the section of Scalar induced gravitational waves and then we discuss how to use the SIGWs to probe PBHs in the section of Searching for PBH DM using SIGWs. Finally, summary and outlook are given in the section of Summary and outlook.

FORMATION OF PBHS

In this section, we will introduce the formation of PBHs and take a brief review on calculating the mass function of PBHs, β. PBHs are generated from the collapse of all the matter inside the Hubble volume. Therefore, there exists a one-to-one correspondence between the mass of PBHs and the comoving frequency f_*, namely Carr and Hawking (1974); Carr (1975).

$$m^*_{\text{pbh}} \approx 2.3 \times 10^{18} M_\odot \left(\frac{3.91}{g^{\text{form}}_*}\right)^{1/6} \left(\frac{H_0}{f_*}\right)^2,$$

(Equation 1)

where g^{form}_* is the corresponding degrees of freedom and H_0 is the Hubble constant by today. Moreover, the one-to-one correspondence can be transferred to another useful form, namely

$$m^*_{\text{pbh}} \approx 2 \times 10^5 M_\odot \left(\frac{t}{1s}\right).$$

(Equation 2)

The fraction of PBHs in all the DM, $f_{\text{pbh}} \equiv \Omega_{\text{PBH}}/\Omega_{\text{DM}}$ can be estimated by Nakama et al. (2017).

$$f_{\text{pbh}} \simeq 2.5 \times 10^8 \beta \left(\frac{g^{\text{form}}_*}{10.75}\right)^{-\frac{1}{4}} \left(\frac{m_{\text{pbh}}}{M_\odot}\right)^{-\frac{1}{2}}.$$

(Equation 3)

On comoving slices, the relation between the primordial comoving curvature perturbation, $\zeta(k)$, and the density contrast, $\Delta(k)$, at linear-order is given by

$$\Delta(k) = \frac{2(1+w)}{5+3w}\left(\frac{k}{aH}\right)^2 \zeta(k),$$

(Equation 4)

where w is the equation of state and H is the Hubble parameter. The comoving curvature perturbation ζ is related to the metric perturbations by

$$\zeta \equiv \psi - \mathcal{H}(v + B),$$

(Equation 5)

where our notations for the scalar perturbations ψ, v, and B are introduced in Equation (3) and Equation (3) below. Moreover, the comoving curvature perturbation is related to the Bardeen potential (see Equation (23) below) by

$$\zeta = \Psi - \frac{2}{3(1+w)}\left(\mathcal{H}^{-1}\Psi' + \Phi\right)$$

(Equation 6)

For adiabatic perturbations, ζ stays constant on superhorizon scales. Then we have $\Phi = -3(1+w)/(5+3w)\zeta$ by assuming the absence of anisotropies and $\Phi = -2/3\zeta$ during RD. The density contrast smoothed over a scale, R, is calculated as

$$\Delta(\boldsymbol{x}, R) = \int \mathrm{d}^3 x' W(|\boldsymbol{x} - \boldsymbol{x}'|, R)\Delta(\boldsymbol{x}'), \quad \Delta(\boldsymbol{k}, R) = W(k, R)\Delta(k), \qquad \text{(Equation 7)}$$

with W to be the window function chosen to smooth the density contrast. The variance of $\Delta(\boldsymbol{k}, R)$ is given by

$$\langle \Delta^2 \rangle = \int_0^\infty \frac{\mathrm{d}k}{k} W^2(k, R) \frac{4(1+w)^2}{(5+3w)^2}(kR)^4 P_\zeta(k), \qquad \text{(Equation 8)}$$

where we define the dimensionless curvature power spectrum as $\langle \zeta(k)\zeta(k') \rangle \equiv \frac{2\pi^2}{k^3}\delta(\boldsymbol{k} + \boldsymbol{k}')P_\zeta(k)$. Usually, the amplitude of perturbations is assumed to obey Gaussian distribution. Once the perturbation satisfies the formation criterion, then PBHs are generated. Therefore, the formation of PBHs can be regarded as the statistics of peaks of a three-dimensional Gaussian random field, also known as peak theory Bardeen et al. (1986). PBHs might be generated by very large perturbations with amplitudes $\mathcal{O}(0.01 - 0.1)$ if PBHs constitute most of the DM in our Universe. As a result, the primordial power spectrum that generate PBHs will have a "bump" on scales much smaller than the CMB scales Ivanov et al. (1994); Garcia-Bellido et al. (1996); Ivanov (1998); Yokoyama (1997); Kawasaki et al. (2006); Hertzberg and Yamada (2018); Inomata et al. (2018, 2017b); Kohri and Terada (2018b). As a benchmark example, we will assume that the power spectrum is "spiky" at a particular scale, k_*, to calculate β. In this case, the production of PBHs is almost monochromatic. Otherwise, for a broad power spectrum, one has taken into account the so-called "cloud-in-cloud" problem where a single PBH is swallowed by the formation of a bigger PBH. Moreover, there are perturbations with different frequency and different amplitudes which may blur the calculation.

For spicky spectrum, using peak theory, the number density of peaks can be approximated by (see e.g., Equation (4.14) in Bardeen et al. (1986))

$$n_{\mathrm{pk}}(\nu_c) \simeq \frac{\left(\langle k^2 \rangle / 3\right)^{3/2}}{(2\pi)^2}\left(\nu_c^2 - 1\right)e^{-\nu_c^2/2}, \qquad \text{(Equation 9)}$$

where the dimensionless threshold is defined as $\nu_c \equiv \Delta_c / \sqrt{\langle \Delta^2 \rangle}$. $\langle k^2 \rangle$ is defined as

$$\langle k^2 \rangle = \frac{1}{\Delta^2}\int_0^\infty \frac{\mathrm{d}k}{k} k^2 W^2(k, R) P_\zeta(k) \qquad \text{(Equation 10)}$$

Moreover, β is related to n_{pk} by $\beta = n_{\mathrm{pk}}(\nu_c)(2\pi)^{3/2}R^3$. Another commonly used method to calculate β is the Press-Schechter formalism, where β is evaluated by simply integrating the probability density function (PDF) beyond the threshold value

$$\beta = \int_{\nu_c}^{+\infty} \frac{\mathrm{d}\nu}{\sqrt{2\pi}}e^{-\nu^2/2} = \frac{1}{2}\mathrm{erfc}\left(\frac{\nu_c}{\sqrt{2}}\right). \qquad \text{(Equation 11)}$$

The Press-Schechter formalism only considers the amplitude of the perturbation but neglecting the higher derivatives. The comparison between Press-Schechter formalism and peak theory can be found in Young et al. (2014), and the result showed close agreement differing by a factor of 10 for large ν_c.

The formation of PBHs depends on many aspects, and there are some potential problems in calculating the mass function of PBHs. We will discuss the relevant aspects next.

Primordial non-gaussianities

Formation of PBHs takes place at the tail of the PDF of the perturbations. Hence any non-Gaussianities that alter the PDF could significantly change the formation probability of PBHs. The impacts of non-Gaussianities on the formation of PBHs have been discussed long ago Bullock and Primack (1997); Ivanov (1998); Pina Avelino (2005); Hidalgo (2007); Klimai and Bugaev (2012). Besides considering a certain inflation model, a commonly used non-Gaussian model is the local-type non-Gaussianities, where the perturbation is expanded by the Gaussian part such that (up to cubic order)

$$\zeta = f(\zeta_g) = \zeta_g + F_{\mathrm{NL}}\left(\zeta_g^2 - \langle \zeta_g^2 \rangle\right) + G_{\mathrm{NL}}\zeta_g^3. \qquad \text{(Equation 12)}$$

Here ζ_g is the Gaussian part whose PDF is Gaussian. The non-Gaussian parameter F_{NL} would skew the PDF and G_{NL} will change the kurtosis of the PDF. Since the Press-Schechter formalism simply integrating the PDF above the threshold value, it is convenient in estimating the mass function β in the presence of

non-Gaussianities. Let P_{NG} to be the PDF of ζ and P_G to be the PDF of the Gaussian part, ζ_g. Then P_{NG} can be obtained by changing the variables, $\zeta_g = f^{-1}(\zeta)$, such that

$$\beta = \int_{\zeta_c}^{\infty} P_{\text{NG}}(\zeta)\mathrm{d}\zeta = \int_{f_i^{-1}(\zeta)>\zeta_c} \sum_{i=1}^{n} \frac{\mathrm{d}f_i^{-1}(\zeta)}{\mathrm{d}\zeta} P_G\left[f_i^{-1}(\zeta)\right]\mathrm{d}\zeta. \qquad \text{(Equation 13)}$$

This is equivalent to integrate the Gaussian PDF in the region, $f_i^{-1}(\zeta)>\zeta_c$. Here, the lower index i indicates the i-th solution of the total n real solutions. In Byrnes et al. (2012), Byrnes et al. used the above method to calculated β within local-type non-Gaussianities up to cubic order. After that, the formation of PBHs within non-Gaussianities was studied up to fifth-order Young and Byrnes (2013) and their results showed a highly sensitive relation between β and non-Gaussian parameters (F_{NL}, G_{NL}, etc.).

Except for changing the variables in Equation (13), Franciolini et al. (2018) adopted another method, the path-integral formulation, to calculate β in non-Gaussian regions. The authors expressed β by the sum of the N-point correlation function. Readers interested in the path-integral formulation can refer to their work and the references therein.

However, the path-integral formulation might be impractical to calculate β. Riccardi et al. argued that the non-Gaussianities would affect cumulants at any order Riccardi et al. (2021). Therefore, to get the exact result for β, one has to sum over all the N-point correlation function, which is impractical. They also proposed a semi-analytical expression to estimate the mass function of PBHs, see Equation (8) in Riccardi et al. (2021).

The non-linear effects between density contrast and curvature perturbation

The standard procedure to calculate the density contrast is based on Equation (4). However, this equation is just the linear relation between the density contrast and the comoving curvature perturbation. In the comoving slicing, the non-linear relation in the long-wavelength approximation is given by Harada et al. (2015); Yoo et al. (2018); Musco (2019).

$$\Delta(r, t) = -\frac{4(1+w)}{5+3w}\left(\frac{1}{aH}\right)^2 e^{-5\zeta(r)/2}\nabla^2 e^{\zeta(r)/2}. \qquad \text{(Equation 14)}$$

Owing to the linear relation, the PDF of density contrast will no longer obey Gaussian distribution even if the PDF of curvature perturbations is Gaussian. This is an unavoidably generated non-Gaussianities that make the PBHs inevitably form in non-Gaussian regions. Recently, these "intrinsic non-Gaussianities" generated by the non-linear effects were studied in Yoo et al. (2018); Kawasaki and Nakatsuka (2019); De Luca et al. (2019b); Young et al. (2019) using either peak theory or Press-Schechter formalism. They found that the "intrinsic non-Gaussianities" would slightly suppress the PBH formation. More precisely, to produce the same abundance of PBH in our Universe, the power spectrum of ζ needs to be amplified by a factor of $\sim \mathcal{O}(2)$ if using the linear relation, Equation (4), to calculate the abundance.

Window function and power spectrum

From Equation (8), it is clear that the formation of PBHs depends on the choice of window functions and the power spectrum of the primordial scalar perturbations. The power spectrum can be given by the inflation model, while the choice of the window function is a coarse-graining procedure. Despite several commonly used window functions in literature, there is no physical interpretation on which window function should be used. The choice of window function will lead to uncertainties in calculating the mass function of PBHs, see Ando et al. (2018a); Young (2019); Tokeshi et al. (2020).

The abundance of PBHs introduced in Equation (9) and Equation (11) can be applied to a narrow power spectrum, where the PBHs are about monochromatic, and one can assume that the PBHs are formed at the same time. However, for a broad power spectrum, PBHs of different masses are expected to be formed at a different time, and the formation process will be rather complicated.

For the broad case, the Press-Schechter formalism failed, and one has to adopt the peak theory to evaluate the results. In Moradinezhad Dizgah et al. (2019); De Luca et al. (2020b), the authors studied the formation of PBHs for a tilted broad power spectrum, namely

$$P_\zeta = A(k/k_s)^{n_p}\Theta(k_s - k)\Theta(k - k_l), \qquad \text{(Equation 15)}$$

where Θ denotes the Heaviside theta function. For a broad and flat spectrum, $n_p=0$, the corresponding mass distribution of PBHs is dominated by a single m_{pbh}. They also found that the mass function has a power-law tail, scaling as $m_{pbh}^{-3/2}$.

Recently, Yoo et al. Yoo et al. (2021) proposed a modified procedure to calculate PBH abundance in which they consider the intrinsic non-Gaussian effects within an arbitrary power spectrum in the absence of primordial non-Gaussianities. The results for a narrow spectrum showed no window function dependence, while the results for a broad power spectrum depends largely on the choice of window functions. They concluded that the top-hat window function in Fourier space would be the best choice since it minimizes the required property in theoretical PBH estimation.

The formation criterion

Studies on the critical value of PBH formation can be traced back since 1975 when Carr first estimated the value of Δ_c by considering simplified Jeans length in Newtonian gravity, $\Delta_c = c_s^2$ Carr (1975), where $c_s = 1/\sqrt{3}$ is the sound speed during RD. However, the exact value of Δ_c is still a debating question since it depends on the initial density profile Polnarev and Musco (2007), the equation of state and the sound speed Jedamzik (1997); Byrnes et al. (2018), primordial non-Gaussianities Kehagias et al. (2019), the primordial scalar power spectrum Germani and Musco (2019) and even the window function Young (2019).

Despite some spherically numeric simulations Jedamzik and Niemeyer (1999); Shibata and Sasaki (1999); Musco et al. (2005); Hawke and Stewart (2002); Polnarev and Musco (2007); Musco et al. (2009); Musco and Miller (2013); Nakama et al. (2014); Harada and Jhingan (2016); Harada et al. (2015); Musco (2019); Escrivà et al. (2020a) on the formation of PBHs, Harada et al. proposed an analytical expression, $\Delta_c = [3(1 + w)/(5 + 3w)]\sin^2[\pi\sqrt{w}/(1 + 3w)] \simeq 0.41$ during RD Harada et al. (2013). Escriva et al. also proposed an approximate expression for Δ_c for $w \in [1/3,1]$ Escrivà et al. (2020b). The analytical Δ_c in a general cosmological background is studied by Escrivà et al. (2020b) where they consider the equation of state to be $w \in (0,1]$.

Recently, Kehagias et al. (2019) estimated the effects of "intrinsic non-Gaussianities" generated by the non-linear relation, Equation (14), on Δ_c. They found that the relative change of Δ_c is at the percent level, which might not be significant due to other uncertainties in estimating the formation of PBHs. More recently, a detailed study based on numeric simulation was made by Musco et al. Musco et al. (2020) where they consider the intrinsic non-Gaussian effects and some commonly used power spectrum that generate the PBHs. They also gave an analytical approach to estimate Δ_c for all possible shapes of the power spectrum, see Equation (19) in Musco et al. (2020).

Apart from using Δ_c, Shibata and Sasaki proposed that the compaction function, which equals to half of the volume average of the density perturbations in the long-wavelength limit, can be used to described the formation of PBHs Shibata and Sasaki (1999). A general definition for the compaction function was introduced in Harada et al. (2015) such that $\mathcal{C} = 2\delta M/R$. Here R represents the areal radius and δM stands for the mass difference between the Misner-Sharp mass insides a sphere of radius r and the mass inside a sphere with the same radius in the FLRW universe.

Using the maximum value of the compaction function, $\mathcal{C}_{max}$, as a formation criterion, there would be less dependence on the shape of the density perturbation Shibata and Sasaki (1999), and this is later confirmed numerically by Harada and Jhingan (2016). Harada and Jhingan (2016) also found that there would be less dependence on the lapse function if using $\mathcal{C}_{max}$ instead of Δ_c. Recently, it was shown in Escrivà et al. (2020a) that the threshold value of compaction function, $\mathcal{C}_{max,c}$, is only sensitive to the curvature at the maximum and $\mathcal{C}_{max,c}$ is, to some approximations, a universal quantity to describe the PBH formation.

SCALAR INDUCED GRAVITATIONAL WAVES

In this section, we will introduce the calculations of SIGWs during RD. Let's begin with the most generic perturbed metric, which contains scalar modes and tensors modes, namely

$$g_{00} = -1 - 2\varphi,$$
$$g_{0i} = a\partial_i B,$$
$$g_{ij} = a^2\delta_{ij} + a^2\left(\frac{1}{2}h_{ij} - 2\delta_{ij}\psi + 2\partial_i\partial_j E\right),$$

(Equation 16)

where φ, B, ψ and E are linear scalar perturbations while the vector perturbations are not considered here. For vector-induced GWs and tensor-induced GWs, we refer the readers to Gong (2019). Here, h_{ij} denotes the second-order tensor mode. We do not consider the first-order tensor mode, since the second-order effects will far exceed the linear-order effects during the formation of PBHs Saito and Yokoyama (2009). During RD, the cosmological background is described by perturbed perfect fluid, which reads

$$
\begin{aligned}
T_{00} &= \rho + 2\rho\varphi + \delta\rho, \\
T_{0i} &= -\rho\partial_i B - P\partial_i v - \rho\partial_i v, \\
T_{ij} &= (P + \delta P)\delta_{ij} - 2P\psi\delta_{ij} + 2P\partial_i\partial_j E,
\end{aligned}
\qquad \text{(Equation 17)}
$$

where v is the velocity potential, P and ρ are the pressure and the energy density of the background while δP and $\delta\rho$ are the corresponding first-order perturbations. Here we neglect the anisotropies caused by neutrinos and photon Saga et al. (2015).

As we shall see, besides the GWs, there is only one physical degree of freedom in our calculation. Consider a first-order change in the coordinate such that

$$
\tilde{\eta} = \eta + T, \tilde{x}^i = x^i + \partial^i L, \qquad \text{(Equation 18)}
$$

and the scalar modes will transform as Malik and Wands (1998).

$$
\begin{aligned}
\tilde{\varphi} &= \varphi + \mathcal{H}T + T', & \text{(Equation 19)} \\
\tilde{\psi} &= \psi - \mathcal{H}T, & \text{(Equation 20)} \\
\tilde{B} &= B - T + L', & \text{(Equation 21)} \\
\tilde{E} &= E + L, & \text{(Equation 22)}
\end{aligned}
$$

where a prime denotes a derivative with respect to the conformal time η. The most generic perturbed metric has four scalar modes. However, one can fix T to determine the time slicing and choose L to decide the spatial coordinates on the hyper-surfaces. This would reduce 2° of freedom. Furthermore, the Einstein equation will reduce one more degree of freedom and give the equation of motion for the last degree of freedom.

The simplest gauge to calculate the SIGWs is the Newton gauge, also known widely as orthogonal zero-shear gauge, longitudinal gauge. Newton gauge demands that $\tilde{B} = \tilde{E} = 0$. This can be done by choosing $L=-E$ and $T = B - E'$. Then, the remaining two modes are just the Bardeen potential

$$
\Phi \equiv \varphi + \mathcal{H}\sigma + \sigma', \quad \Psi \equiv \psi - \mathcal{H}\sigma, \qquad \text{(Equation 23)}
$$

where $\sigma \equiv E' - B$ is the shear potential. The advantage of the Newton gauge is that the degrees of freedom are completely fixed, and there are no more gauge modes. The only modes left are just the Bardeen potential $\varphi = \Phi$ and $\psi = \Psi$. Write down the first-order Einstein equation in terms of the Bardeen potential, one finds that $\Phi = \Psi$ and the equation of motion for the only scalar mode left is

$$
\Phi'' + 4\mathcal{H}\Phi - \frac{1}{3}\nabla^2\Phi = 0. \qquad \text{(Equation 24)}
$$

Keeping the decay modes of Equation (24), the solution of Φ in Fourier space is given by

$$
\Phi(\boldsymbol{k}, \eta) \equiv \Phi_k T_\Phi(k\eta) = \Phi_k \frac{9}{x^2}\left(\frac{\sin\left(x/\sqrt{3}\right)}{x/\sqrt{3}} - \cos\left(x/\sqrt{3}\right)\right), \qquad \text{(Equation 25)}
$$

where we label the primordial value as Φ_k and T_Φ is the normalized transfer function such that $T_\Phi(0) = 1$. We also introduce the dimensionless variable $x \equiv k\eta$. The value of Φ_k is given by certain inflation models and we will treat it as free parameters in our discussion. Moreover, the first-order GWs is given by

$$
h''^{(1)}_{ij} + 2\mathcal{H}h'^{(1)}_{ij} - \nabla^2 h^{(1)}_{ij} = 0, \qquad \text{(Equation 26)}
$$

which is a source-free equation. The linear GWs will decay from the primordial value as η^{-1} during RD. During the formation of PBHs, the scalar power spectrum are enhanced to $\mathcal{O}(0.01)$ if PBH represents the main part of the DM. In this case, the second-order SIGWs would be stronger than the linear GWs, and hence we will not consider $h^{(1)}_{ij}$. Readers interested in second-order GWs induced by $h^{(1)}_{ij}$ can refer to Gong (2019).

Up to second-order, the evolution of the GWs can be written as

$$h_{ij}'' + 2\mathcal{H}h_{ij}' - \nabla^2 h_{ij} = -4\mathcal{T}_{ij}^{\ell m}S_{\ell m}, \tag{Equation 27}$$

where $\mathcal{T}_{ij}^{\ell m} = e_{ij}^{(+)}(\mathbf{k})e^{(+)lm}(\mathbf{k}) + e_{ij}^{(\times)}(\mathbf{k})e^{(\times)lm}(\mathbf{k})$ is the transverse and traceless projection operator. The polarization tensors are defined as $(e_i e_j - \overline{e}_i\overline{e}_j)/\sqrt{2}$ and $(e_i\overline{e}_j + \overline{e}_i e_j)/\sqrt{2}$ for + and × modes. Here, we choose $e=(1,0,0)$, $\overline{e}=(0,1,0)$ and $\mathbf{k}=(0,0,k)$.

The source term in Equation (27) reads

$$S_{ij} = 3\Phi\partial_i\partial_j\Phi - \frac{2}{\mathcal{H}}\partial_i\Phi'\partial_j\Phi - \frac{1}{\mathcal{H}^2}\partial_i\Phi'\partial_j\Phi', \tag{Equation 28}$$

where we have expressed the density perturbation $\delta\rho$, the velocity potential v and the pressure perturbation δP in terms of the scalar modes Φ. Overall, the perfect fluid acts like an intermediary, and the GWs seem to be generated by the scalar modes. This is why SIGWs gain its name. Equation (27) can be solved by Green's function in Fourier space, namely

$$h(\eta, \mathbf{k}) = \frac{1}{a(\eta)}\int_0^\eta g_k(\eta;\eta')a(\eta')S(\eta',\mathbf{k})d\eta'. \tag{Equation 29}$$

We define $S(\eta,\mathbf{k}) \equiv -4e^{ij}(\mathbf{k})\mathcal{S}(\eta,\mathbf{k})$ and $\mathcal{S}(\eta,\mathbf{k})$ is the source term transferred to Fourier space. Here, we define the Fourier transform of h_{ij} to be

$$h_{ij}(\eta, \mathbf{x}) = \int\frac{d^3k}{(2\pi)^3}\left[h^{(+)}(\eta,\mathbf{k})e_{ij}^{(+)}(\mathbf{k}) + h^{(\times)}(\eta,\mathbf{k})e_{ij}^{(\times)}(\mathbf{k})\right]e^{i\mathbf{k}\cdot\mathbf{x}}. \tag{Equation 30}$$

In the following part, we write $h(\eta,\mathbf{k})$ to denote either the plus mode or the cross mode. In our convention, $S(\eta,\mathbf{k})$ takes the form

$$S(\eta,\mathbf{k}) = -4\int\frac{d^3p}{(2\pi)^{3/2}}\left(e^{ij}p_ip_j\right)\Phi_p\Phi_{|p-k|}F(|\mathbf{p}|,|\mathbf{k}-\mathbf{p}|,\eta). \tag{Equation 31}$$

The transfer function is defined as

$$F(u,v,x) = 3T_\varphi(ux)T_\varphi(vx) + uxT_\varphi'(ux)T_\varphi(vx) + vxT_\varphi'(vx)T_\varphi(vx) + uvx^2T_\varphi'(ux)T_\varphi'(vx). \tag{Equation 32}$$

For convenience, we introduce the dimensionless variable $u\equiv p/k$, $v\equiv|\mathbf{p}-\mathbf{k}|/k$ and $x\equiv k\eta$. Unless otherwise being stated, the prime with $T'(y)$ denotes the derivative with respect to y, other than the conformal time. The Green's function in Equation (29) takes the form $g_k(\eta;\eta') = \frac{1}{k}\sin(k\eta - k\eta')$ during RD. A more important quantity in observation is the density parameter of the stochastic GW background defined as the energy of GWs per logarithm frequency normalized by the critical energy $\rho_c(\eta)$

$$\Omega_{GW}(k,\eta) \equiv \frac{1}{\rho_c}\frac{d\rho_{GW}}{d\ln k} = \frac{k^3}{48\pi^2}\left(\frac{k}{\mathcal{H}}\right)^2\overline{\langle|h(\eta,k)|^2\rangle}, \tag{Equation 33}$$

where the overline denotes the oscillating average. To calculate the stochastic GW background of the SIGWs, we have to know the primordial scalar power spectrum, which is given by specific inflation models. In this paper, we do not consider certain inflation model, instead, we will parameterize the power spectrum by some commonly used function in literature. The density parameter is evaluated as (see e.g. Kohri and Terada (2018a))

$$\begin{aligned}
\Omega_{GW}(k,\eta) &= \left(\frac{k}{\mathcal{H}}\right)^2\frac{k^3}{48\pi^2 a(\eta)^2}\int d\tilde\eta_1 d\tilde\eta_2 g_k(\eta;\tilde\eta_1)g_{k'}(\eta;\tilde\eta_2)a(\tilde\eta_1)a(\tilde\eta_2)\langle S(\tilde\eta_1,\mathbf{k})S(\tilde\eta_2,\mathbf{k'})\rangle.\\
&= \left(\frac{k}{\mathcal{H}}\right)^2\frac{4\pi^2 k^3}{3a(\eta)^2}\int\frac{d^3p}{(2\pi)^3}\int d\tilde\eta_1 d\tilde\eta_2 a(\tilde\eta_1)a(\tilde\eta_2)g_k(\eta;\tilde\eta_1)g_k(\eta;\tilde\eta_2)\left(e^{ij}p_ip_j\right)^2\frac{1}{p^3|\mathbf{k}-\mathbf{p}|^3}\\
&\quad\times P_\Phi(k)P_\Phi(|\mathbf{k}-\mathbf{p}|)\left[F(|\mathbf{p}|,|\mathbf{k}-\mathbf{p}|,\tilde\eta_1)F(|\mathbf{p}|,|\mathbf{k}-\mathbf{p}|,\tilde\eta_2) + F(|\mathbf{p}|,|\mathbf{k}-\mathbf{p}|,\tilde\eta_1)F(|\mathbf{k}-\mathbf{p}|,|\mathbf{p}|,\tilde\eta_2)\right]\\
&= \left(\frac{k}{\mathcal{H}}\right)^2\frac{8\pi^2 k}{3}\int\frac{d^3p}{(2\pi)^3}\left(\int_0^\eta d\tilde\eta_1\frac{a(\tilde\eta_1)}{a(\eta)}kg_k(\eta;\tilde\eta_1)\tilde F(|\mathbf{p}|,|\mathbf{k}-\mathbf{p}|,\tilde\eta_1)\right)^2\left(e^{ij}p_ip_j\right)^2\frac{1}{p^3|\mathbf{k}-\mathbf{p}|^3}\\
&\quad\times P_\Phi(k)P_\Phi(|\mathbf{k}-\mathbf{p}|)\\
&\simeq \frac{1}{6}\int_0^\infty du\int_{|1-u|}^{1+u}dv\frac{v^2}{u^2}\left[1 - \left(\frac{1+v^2-u^2}{2v}\right)^2\right]^2 P_\Phi(uk)P_\Phi(vk)\overline{I^2(u,v,x)},
\end{aligned}$$

$$\tag{Equation 34}$$

where in the last step of Equation (34), we define the power spectrum as

$$\langle \Phi(\boldsymbol{k})\Phi(\boldsymbol{k'})\rangle \equiv \frac{2\pi^2}{k^3}P_\Phi(k)\delta(\boldsymbol{k}+\boldsymbol{k'}), \qquad \text{(Equation 35)}$$

and the kernel function to be

$$I(u,v,x) \equiv \int_0^x \mathrm{d}\tilde{x}\tilde{x}\sin(x-\tilde{x})\tilde{F}(u,v,x), \qquad \text{(Equation 36)}$$

where $\tilde{F}(u,v,x) \equiv (F(u,v,x)+F(v,u,x))/2$ is the symmetric part of the transfer function. We also used that $\mathcal{H} = \eta^{-1}$ and $a(\tilde{\eta})/a(\eta) = \tilde{\eta}/\eta$ during RD. We sum over the two polarization modes in Equation (34) and the e^{ij} in the expression refers to either the "+" mode or the "×" mode. In the last step of Equation (34), the overline denotes the oscillating average, namely $\sin^2 x \to \frac{1}{2}$, $\cos^2 x \to \frac{1}{2}$ and $\sin x \cos x \to 0$. The Ω_{GW} has a time dependence through $I(u,v,x)$ and, as we will demonstrate below, the function $I(u,v,x)$ will converge to a finite value at late time.

The density parameter given by Equation (34) is independent of the position, rendering the SIGWs are isotropic GWs. This is due to the statistical homogeneity of the FLRW metric. However, the GW detectors would detect GWs from different directions, resulting in angular anisotropies of the SIGW signal. This was studied in Bartolo et al. (2020). In the absence of primordial non-Gaussianities, the authors found that the anisotropies are negligible by today due to the propagation effects.

After the horizon entry, the energy of GWs redshift as radiation, $\rho_{\mathrm{GW}} \propto a^{-4}$. Therefore, the current GW density parameter, $\Omega_{\mathrm{GW},0}$ would be

$$\Omega_{\mathrm{GW},0}(\eta_0,f) = \Omega_r\Omega_{\mathrm{GW}}(\eta_c,f), \qquad \text{(Equation 37)}$$

where Ω_r is the energy density fraction of radiation by today, and we neglect the effects of relativistic degrees of freedom. Here, $\Omega_{\mathrm{GW}}(\eta_c,f)$ is the late time value when $\Omega_{\mathrm{GW}}(\eta,f)$ becomes a constant and can be computed by taking $I(u,v,x\to\infty)$ (Here, a constant means that $\Omega_{\mathrm{GW}}(\eta,f)$ is independent of time). This result would be more clear if one considers the evolution of tensor modes during both MD and RD. See e.g., Kohri and Terada (2018a) where the author studied analytically the SIGWs during MD, RD and RD-to-MD transition. The analytical expression for $\overline{I^2(u,v,x)}$ was derived in Espinosa et al. (2018); Kohri and Terada (2018a). The indefinite integral of Equation (36) is given by

$$
\begin{aligned}
I(u,v,x) = & -\frac{27(u^2+v^2-3)^2}{16u^3v^3}\Bigg\{\left[\mathrm{Si}\left(\left(1-\frac{(u+v)}{\sqrt{3}}\right)x\right) + \mathrm{Si}\left(\left(1+\frac{(u+v)}{\sqrt{3}}\right)x\right)\right.\\
& \left. -\mathrm{Si}\left(\left(1+\frac{(u-v)}{\sqrt{3}}\right)x\right) - \mathrm{Si}\left(\left(1-\frac{(u-v)}{\sqrt{3}}\right)x\right)\right]\cos x + \left[\mathrm{Ci}\left(\left(1+\frac{(u-v)}{\sqrt{3}}\right)x\right)\right.\\
& \left. + \mathrm{Ci}\left(\left(1-\frac{(u-v)}{\sqrt{3}}\right)x\right) - \mathrm{Ci}\left(\left|1-\frac{(u+v)}{\sqrt{3}}\right|x\right) - \mathrm{Ci}\left(\left(1+\frac{(u+v)}{\sqrt{3}}\right)x\right)\right]\sin x + \frac{1}{u^2+v^2-3}\\
& \times \left(4uv + \left(u^2+v^2-3\right)\ln\left|1-\frac{4uv}{(u+v)^2-3}\right|\right)\sin x + \frac{12}{x^2(u^2+v^2-3)^2}\\
& \times \left[2u\cos\frac{ux}{\sqrt{3}}\left(vx\cos\frac{vx}{\sqrt{3}} - \sqrt{3}\sin\frac{vx}{\sqrt{3}}\right) + 2u\left(-vx + \sqrt{3}\sin\frac{vx}{\sqrt{3}}\right)\right.\\
& \left. + \sin\frac{ux}{\sqrt{3}}\left(2\sqrt{3}v - 2\sqrt{3}v\cos\frac{vx}{\sqrt{3}} + \left(u^2+v^2-3\right)x\sin\frac{vx}{\sqrt{3}}\right)\right]\Bigg]\Bigg\}
\end{aligned}
$$

$$\text{(Equation 38)}$$

Then the late time expression, $\overline{I^2(u,v,x\to\infty)}$, takes the form

$$\overline{I^2} = \frac{729(u^2+v^2-3)^2}{512u^6v^6}\left\{\left(-4uv + (u^2+v^2-3)\ln\left|\frac{3-(u+v)^2}{3-(u-v)^2}\right|\right)^2 + \pi^2(u^2+v^2-3)^2\Theta\left(u+v-\sqrt{3}\right)\right\}. \qquad \text{(Equation 39)}$$

Below we use the comoving curvature perturbation ζ, which has the relation $\zeta = (3/2)\Phi$ to calculate the SIGWs. A widely used model for the power spectrum is the infinite narrow spectrum

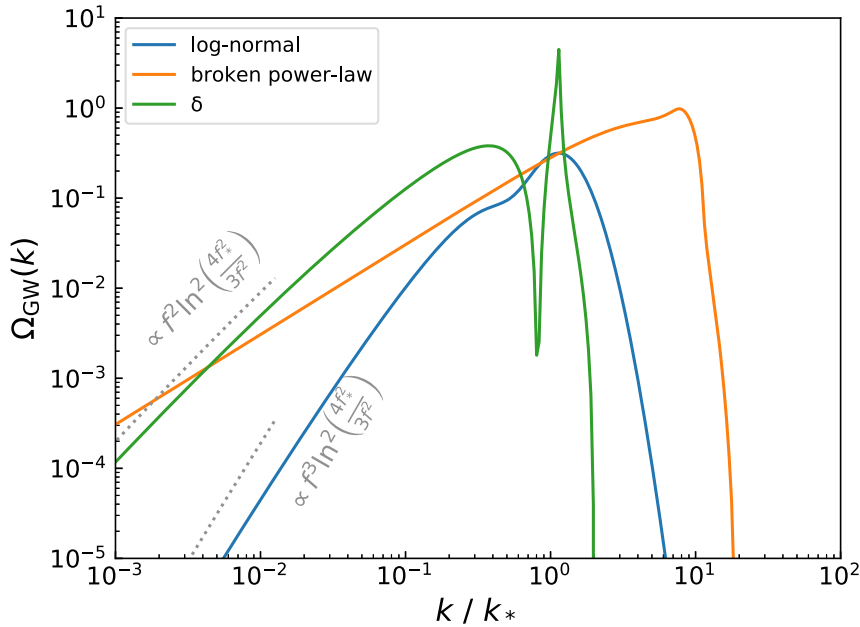$$P_\zeta(k) = Ak_*\delta(k-k_*), \qquad \text{(Equation 40)}$$

Figure 1. SIGWs generated by different power spectrum

The parameters for the log-normal spectrum is $\sigma_* = 0.5$. For the box spectrum, we set $k_{min} = 0.1$ and $k_{max} = 3$.

with a dimensionless amplitude A peaked at k_*. This power spectrum corresponds to a monochromatic PBH formation and is convenient to study the properties of SIGWs from PBHs. For this spectrum, the density parameter has an analytical form, namely

$$\Omega_{GW}(k) = \frac{3A^2\Omega_r}{64}\tilde{k}^2\left(1 - \frac{\tilde{k}^2}{4}\right)^2\left(2 - 3\tilde{k}^2\right)^2\Theta\left(2 - \tilde{k}\right)\left(\left(2 - 3\tilde{k}^2\right)^2\pi^2\Theta\left(2 - \sqrt{3}\,\tilde{k}\right)\right.$$
$$\left. + \left(-4 + \left(2 - 3\tilde{k}^2\right)\ln\left|1 - \frac{4}{3\tilde{k}^2}\right|\right)^2\right),$$

(Equation 41)

where we define $\tilde{k} \equiv k/k_*$. Another example is a log-normal power spectrum parameterized by

$$P_\zeta(k) = \frac{A}{\sqrt{2\pi\sigma_*^2}}\exp\left(-\frac{\ln\tilde{k}^2}{2\sigma_*^2}\right),$$

(Equation 42)

where σ_* is a dimensionless parameter which denotes the width of the power spectrum. The SIGWs generated by this power spectrum has been carefully studied in Pi and Sasaki (2020).

Finally, we consider a box spectrum described by

$$P_\zeta(k) = \frac{A}{\ln\left(\frac{k_{max}}{k_{min}}\right)}\Theta\left(\tilde{k} - k_{min}\right)\Theta\left(k_{max} - \tilde{k}\right).$$

(Equation 43)

In the above case, we have normalized the power spectrum so that $\int P_\zeta(k)\,\mathrm{d}\ln k = A = \langle\zeta^2\rangle$ is the variance of the perturbations. The $\Omega_{GW}(k)$ for these three power spectrum is given in Figure 1.

As shown in the figure, on small scales, the SIGWs will have a cutoff wavelength. The cutoff is due to the momentum conservation such that two modes $\mathbf{k}_1$ and $\mathbf{k}_2$ generate a mode with $\mathbf{k} = \mathbf{k}_1 + \mathbf{k}_2$. Therefore, for a power spectrum defined on $[k_{min}, k_{max}]$, the cutoff wavelength of the corresponding SIGWs will be $2k_{max}$. Since a constant gravitational potential will not change the distribution of matter, it will not induce GWs. After the perturbation re-enters the horizon at $k \simeq k_*$, they will induce GWs, and the shape of Ω_{GW} is dominated by the power spectrum. For instance, a power spectrum with a peak located at k_* will induce GWs with a peak at $2k_*/\sqrt{3}$ where $1/\sqrt{3}$ comes from the sound of speed during RD while a box spectrum will
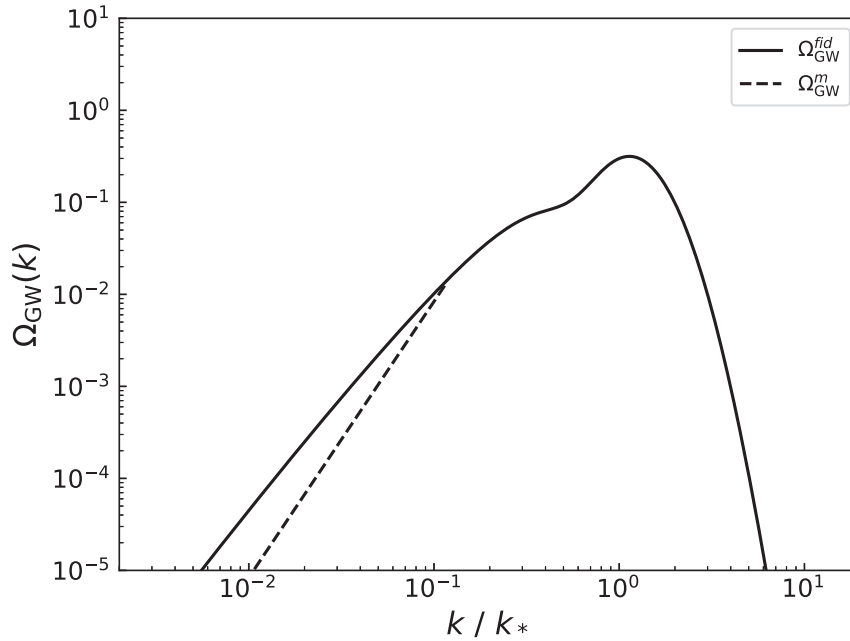
Figure 2. The two models described by Equation (44)

Both lines correspond to the SIGWs induced by a log-normal power spectrum with $\sigma_* = 0.5$. The solid line is the full numeric result, while the dashed line has a k^3 scaling in the infrared region, $k < 0.1 k_*$.

induce a smooth signal. Finally, on large scales, the scaling of SIGWs shows a log-dependent behavior, $\Omega_{GW} \propto f^2 \ln\left(\frac{4f_*^2}{3f^2}\right)$ or $\Omega_{GW} \propto f^3 \ln\left(\frac{4f_*^2}{3f^2}\right)$ where f_* is a pivot scale of the power spectrum. On large scales, the power spectrum has decreased to negligible value, and the signal is dominated by the evolution of scalar perturbations. A strict proof of the log-dependent scaling is given in Yuan et al. (2019b) for a general spectrum. This special scaling is very important in distinguishing the signal of SIGWs from other stochastic GW background, and it could be smoking guns in detecting SIGWs. In Yuan et al. (2019b), Yuan et al. estimated the distinguishability of LISA. They consider a fiducial case, $\Omega_{GW}^{fid}(k)$, generated by a log-normal power spectrum with $\sigma_* = 0.5$ and the other one is described by

$$\Omega_{GW}^m(k) = \begin{cases} \Omega_{GW}^{fid}(0.1k_*)\left(\dfrac{k}{0.1k_*}\right)^3 , & \text{for } k < 0.1k_* , \\ \\ \Omega_{GW}^{fid}(k) , & \text{for } k \geq 0.1k_* . \end{cases} \qquad \text{(Equation 44)}$$

These two cases have different scalings in the infrared region, as shown in Figure 2. A statistic quantity, $\delta\chi^2$, which characterize the discrepancy of two models, takes the form Kuroyanagi et al. (2018).

$$\delta\chi^2 \simeq T \int_0^\infty df \left(\frac{\Omega_{GW}^{fid} - \Omega_{GW}^m}{\Omega_{GW}^m + \Omega_n}\right)^2 , \qquad \text{(Equation 45)}$$

where T is the observation time and Ω_n is the noise density parameter of the detector. Scanning the mass of PBHs, the result of $\delta\chi^2$ is Figure 3. It is shown that LISA can well distinguish the scaling of two models beyond 5σ in a wide mass range, especially for those PBHs of $m_{pbh} \in [10^{-16}, 10^{-14}] \cup [10^{-13}, 10^{-12}] M_\odot$ which could still represent all the DM in our Universe. To summarize, the log-dependent scaling, $\Omega_{GW} \propto f^2 \ln\left(\frac{4f_*^2}{3f^2}\right)$ or $\Omega_{GW} \propto f^3 \ln\left(\frac{4f_*^2}{3f^2}\right)$ can be smoking guns in detecting SIGWs.

Since there are no observational results concerning the primordial scalar power spectrum on small scales, the power spectrum is usually parameterized by some given function in literature. A more realistic way is to
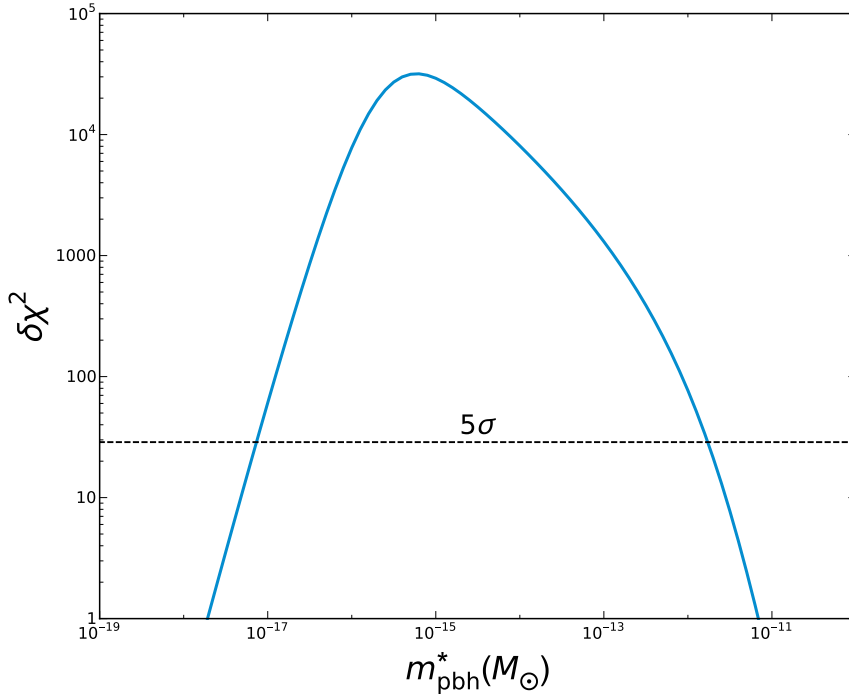
Figure 3. The relation between $\delta\chi^2$ and the peak mass of PBHs (m^*_{pbh} corresponds to k_*) generated by the log-normal power spectrum given in Equation (42) with σ_*=0.5

The amplitude of A is fixed by assuming PBHs represent 10^{-3} of DM. The 5σ dashed line corresponds to $\delta\chi^2 = 28.74$. Taken from Figure 3 in Yuan et al. (2019b).

consider the primordial power spectrum from a given inflation model and then calculate the corresponding SIGWs. See relevant works Kawasaki et al. (2013); Choudhury and Mazumdar (2014); Inomata et al. (2017a); Di and Gong (2018); Ando et al. (2018b, 2018c); Xu et al. (2020); Özsoy and Tasinato (2020); Gao and Yang (2019); Lin et al. (2020); Ballesteros et al. (2020); Liu et al. (2020); Braglia et al. (2020a); Fu et al. (2020); Dalianis and Kritos (2021); Yi et al. (2020a); Dalianis (2020); Aldabergenov et al. (2021); Ragavendra et al. (2020a); Bhaumik and Jain (2020); Zhou et al. (2020); Ragavendra et al. (2020b); Yi et al. (2020b); Braglia et al. (2020b); Gao et al. (2020); Gao (2021).

SIGWs in a general cosmological background

For a constant equation of state and let $c_s^2 = w$, the semi-analytical solutions of SIGWs were obtained by Domènech in Domènech (2019) for $0 < w \leq 1$. Then, the results for constant w were extended to $w < 0$ in Domènech et al. (2020b). For the most general situation where w and c_s^2 may varied, there are no semi-analytical solutions to SIGWs, and a numeric method should be adopted. For instance, during the QCD phase transition, w and c_s^2 may become slightly smaller than 1/3 and the equation $c_s^2 = w$ no longer holds. The SIGWs generated during the QCD epoch were numerically calculated in Abe et al. (2020). The derivation within a general $w(\eta)$ and $c_s(\eta)$ differs from that in RD in the following aspects.

Firstly, the equation of motion for linear scalar perturbations become

$$\Phi'' + 3\mathcal{H}(\eta)\left(1 + c_s^2\right)\Phi' + 3\mathcal{H}^2\left(c_s^2 - w\right)\Phi - c_s^2\nabla^2\Phi = 0, \qquad \text{(Equation 46)}$$

where the conformal Hubble parameter now become $\mathcal{H}(\eta) = \frac{2}{(1+3w)\eta}$. This equation should be numerically solved with the initial condition to be $\Phi_k(\eta \to 0) = \Phi_k T_\Phi(k\eta \to 0) = \Phi_k$.

Secondly, the equation of motion for the second-order tensor modes takes the same form as (Equation 27) but the source term changes to

$$S_{ij} = 2\Phi\partial_i\partial_j\Phi - \frac{4}{3(1+w)}\left(\partial_i\Phi + \frac{\partial_i\Phi'}{\mathcal{H}(\eta)}\right)\left(\partial_j\Phi + \frac{\partial_j\Phi'}{\mathcal{H}(\eta)}\right). \qquad \text{(Equation 47)}$$
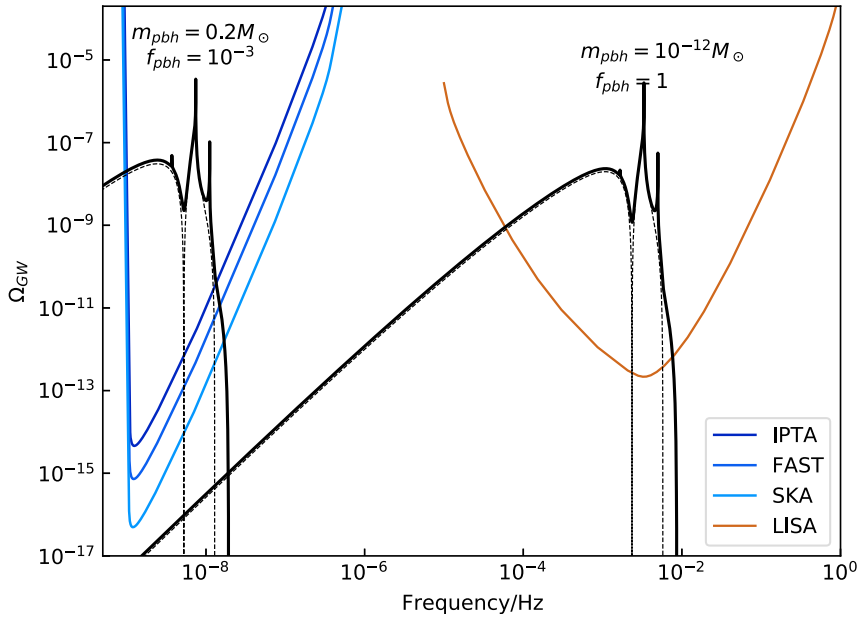
Figure 4. The energy density parameter of SIGWs generated by a δ-spectrum up to third-order
The sensitivity curves for LISA, IPTA, FAST, and SKA are shown. The dashed lines denote the second-order SIGWs, and the solid black lines include the third-order correction. Taken from Figure 1 in Yuan et al. (2019a).

The Green's function and the transfer function methods can still be applied to solve h_{ij}. Since the form of the equation of motion for h_{ij} is unchanged, the solution to h_{ij} takes the same form as Equation (29) except for the Green's function, which now satisfies the equation

$$\left(\partial_\eta^2 + k^2 - \frac{1 - 3w(\eta)}{2}\mathcal{H}^2\right)g_k(\eta, \tilde{\eta}) = \delta(\eta - \tilde{\eta}),$$ (Equation 48)

The solution of $g_k(\eta, \tilde{\eta})$ can be obtained by

$$g_k(\eta, \tilde{\eta}) = \frac{u(\eta)v(\tilde{\eta}) - u(\tilde{\eta})v(\eta)}{u'(\tilde{\eta})v(\tilde{\eta}) - u(\tilde{\eta})v'(\tilde{\eta})},$$ (Equation 49)

with $u(\eta)$ and $v(\eta)$ to be the two independent homogeneous solutions. Move on to the density parameter, the final expression for Ω_{GW} takes the same form as the last line of Equation (34) but the kernel function should now be evaluated as

$$I(u, v, x) = k^2 \int_0^\eta d\tilde{\eta}\frac{a(\tilde{\eta})}{a(\eta)}g_k(\eta, \tilde{\eta})\tilde{F}(|\boldsymbol{p}|, |\boldsymbol{k} - \boldsymbol{p}|, \tilde{\eta}).$$ (Equation 50)

After calculating the oscillating average of $I(u,v,x)$, the density parameter, Ω_{GW}, can be obtained. Readers interested in numerically solutions may refer to Abe et al. (2020) for details where the authors introduce some technique to reduce the computational complexity. The Ω_{GW} of SIGWs generated during the QCD phase transition is shown in Figure 4 in Abe et al. (2020) for a delta-power spectrum.

Higher-order corrections to SIGWs
SIGWs are generated at second-order soured by linear scalar perturbations, which lead to $h_{ij} \sim \Phi^2$. Given that the scalar perturbations are enhanced to $\sim \mathcal{O}(0.01 - 0.1)$ during the formation of PBHs, the higher-order corrections to SIGWs are expected to be significant. The higher-order corrections to SIGWs were first calculated by Yuan et al. where they proposed a semi-analytical method to evaluate the SIGWs generated by a δ-spectrum during RD Yuan et al. (2019a). Yuan et al. computed the tensor modes sourced by the

quadratic, cubic, and biquadratic terms of the linear perturbations during RD. Here we give the source term in Newton gauge up to fourth-order in general cosmological background. Our convention for the higher-order tensor modes are (up to fourth-order)

$$\delta g_{ij} = a^2 \left((1 - 2\Phi)\delta_{ij} + \frac{1}{2}\left(h_{ij}^{(2)} + h_{ij}^{(3)} + h_{ij}^{(4)}\right) \right), \qquad \text{(Equation 51)}$$

and the perturbed perfect fluid up to third-order in Newton gauge is given by

$$T_{00}^{(2)} = \frac{1}{2}\delta\rho^{(2)} + 2\delta\rho^{(1)}\Phi^{(1)} + \rho\Phi^{(2)} + (P+\rho)v_k^{(1)}v^{k(1)}$$

$$T_{0i}^{(2)} = \frac{1}{2}\left(-\rho B_i^{(2)} - 2\delta\rho^{(1)}B_i^{(1)} - 2\left(\delta P^{(1)} + \delta\rho^{(1)}\right)v_i^{(1)} - (P+\rho)\left(4h_{ik}^{(1)}v^{k(1)} + 2\left(\Phi^{(1)} - 2\Psi^{(1)}\right)v_i^{(1)} + v_i^{(2)}\right)\right)$$

$$T_{ij}^{(2)} = Ph_{ij}^{(2)} + 2h_{ij}^{(1)}\delta P^{(1)} + (P+\rho)\left(B_i^{(1)} + v_i^{(1)}\right)\left(B_j^{(1)} + v_j^{(1)}\right) + \frac{1}{2}\delta_{ij}\left(\delta P^{(2)} - 4\delta P^{(1)}\Psi^{(1)} - 2P\Psi^{(2)}\right)$$

$$T_{00}^{(3)} = \left(\delta P^{(1)} + \delta\rho^{(1)}\right)v_k^{(1)}v^{k(1)} + (P+\rho)v^{k(1)}v_k^{(2)} + 2(P+\rho)h_{lm}^{(1)}v^{l(1)}v^{m(1)} + \frac{1}{6}\delta\rho^{(3)} + \frac{1}{3}\rho\Phi^{(3)}$$

$$+ 2(P+\rho)\Phi^{(1)}v_k^{(1)}v^{k(1)} + \delta\rho^{(2)}\Phi^{(1)} + \delta\rho^{(1)}\Phi^{(2)} - 2(P+\rho)\Psi^{(1)}v_k^{(1)}v^{k(1)}$$

$$T_{0i}^{(3)} = \frac{1}{6}\Bigg[(P+\rho)\Bigg[-6B_i^{(1)}B^{k(1)}v_k^{(1)} - 6\left(h_{ik}^{(2)}v^{k(1)} + h_{ik}^{(1)}v^{k(2)}\right) + v_i^{(3)}$$

$$-3\left(\left(2B_i^{(1)} + v_i^{(1)}\right)v_k^{(1)}v^{k(1)} + 4h_{ik}^{(1)}v^{k(1)}\Phi^{(1)} + v_i^{(2)}\left(\Phi^{(1)} - 2\Psi^{(1)}\right) - v_i^{(1)}\left(\left(\Phi^{(1)}\right)^2 - \Phi^{(2)} + 4\Phi^{(1)}\Psi^{(1)} + 2\Psi^{(2)}\right)\right)$$

$$-3\left(\delta P^{(1)} + \delta\rho^{(1)}\right) \times \left(4h_{ik}^{(1)}v^{k(1)} + v_i^{(2)} + 2v_i^{(1)}\left(\Phi^{(1)} - 2\Psi^{(1)}\right)\right) - 3\left(\delta P^{(2)} + \delta\rho^{(2)}\right)v_i^{(1)}$$

$$-3\left(B_i^{(2)}\delta\rho^{(1)} + B_i^{(1)}\delta\rho^{(2)}\right) - \rho B_i^{(3)}\Bigg]$$

$$T_{ij}^{(3)} = \frac{1}{6}\Bigg(2h_{ij}^{(3)}P + 6\left(h_{ij}^{(2)}\delta P^{(1)} + h_{ij}^{(1)}\delta P^{(2)}\right) + 6\left(\delta P^{(1)} + \delta\rho^{(1)}\right)v_i^{(1)}v_j^{(1)}$$

$$+ 3\left(P+\rho\right)\Bigg[v_i^{(1)}B_j^{(2)} + 4h_{jk}^{(1)}v^{k(1)}v_i^{(1)} + v_i^{(1)}v_j^{(2)} + v_j^{(1)}\left(B_i^{(2)} + 4h_{ik}^{(1)}v^{k(1)} + v_i^{(2)} - 8v_i^{(1)}\Psi^{(1)}\right)\Bigg]$$

$$+ 3B_j^{(1)}\Bigg[2\left(B_i^{(1)} + v_i^{(1)}\right)\left(\delta P^{(1)} + \delta\rho^{(1)}\right)$$

$$+ (P+\rho) \times \left(B_i^{(2)} + 4h_{ik}^{(1)}v^{k(1)} + v_i^{(2)} - 4B_i^{(1)}\Phi^{(1)} - 2v_i^{(1)}\left(\Phi^{(1)} + 2\Psi^{(1)}\right)\right)\Bigg]$$

$$+ 3B_i^{(1)}\Bigg[2v_j^{(1)}\left(\delta P^{(1)} + \delta\rho^{(1)}\right) + (P+\rho)\left(B_j^{(2)} + 4h_{jk}^{(1)}v^{k(1)} + v_j^{(2)} - 2v_j^{(1)}\left(\Phi^{(1)} + 2\Psi^{(1)}\right)\right)\Bigg]$$

$$+ \delta_{ij}\Big[\delta P^{(3)} - 2P\Psi^{(3)} - 6\left(\delta P^{(1)}\Psi^{(2)} + \delta P^{(2)}\Psi^{(1)}\right)\Big]\Bigg) \qquad \text{(Equation 52)}$$

where $v_i \equiv v_i^\perp + \partial_i v$ and B_i are the velocity perturbation and vector perturbation in Newton Gauge, respectively.

The equation of motion for each $h_{ij}^{(n)}$ takes the same form as Equation (27) and the third-order source term reads

$$S_{ij}^{(3)} = -\frac{4}{9\mathcal{H}^4(1+w)^2}\left\{(\mathcal{H}\partial_i\Phi + \partial_i\Phi')(\mathcal{H}\partial_j\Phi + \partial_j\Phi')\left[-2(1+c_s^2)\partial^2\Phi + 6\mathcal{H}^2(c_s^2 - w)\Phi\right.\right.$$
$$\left.\left. + 3\mathcal{H}(3 + 2c_s^2 + w)\Phi'\right] + 3\mathcal{H}(1+w)(4\mathcal{H}\Phi - \Phi')\partial_i\Phi'\partial_j\Phi' - 3\mathcal{H}^3(1+w)(2\mathcal{H}(5+3w)\Phi - \Phi')\partial_i\Phi\partial_j\Phi\right\}$$

(Equation 53)

and the fourth-order source term is given by

$$S_{ij}^{(4)} = 16\Phi^3\partial_i\partial_j\Phi - \frac{4}{27\mathcal{H}^6(1+w)^3}\left\{(\mathcal{H}\partial_i\Phi + \partial_i\Phi')(\mathcal{H}\partial_j\Phi + \partial_j\Phi')\left[4(1+c_s^2)^2(\partial^2\Phi)^2\right.\right.$$

$$-\mathcal{H}^2(9 + 5c_s^2 + 9w + 9wc_s^2)\partial_k\varphi\partial^k\Phi + 4c_s^2(2\mathcal{H}\partial^k\Phi + \partial^k\Phi')\partial_k\Phi'$$

$$-6\mathcal{H}(1+c_s^2)(2\mathcal{H}(3 + 2c_s^2 + w)\Phi + (5 + 4c_s^2 + w)\Phi')\partial^2\Phi$$

$$+18\mathcal{H}^3(7 + 4c_s^4 + 7c_s^2 - wc_s^2 + 7w + 4w^2)\Phi\Phi'$$

$$+36\mathcal{H}^4(1 + c_s^4 - 2wc_s^2 + 2w + 2w^2)\Phi^2 + 9\mathcal{H}^2(1 + c_s^2)(5 + 4c_s^2 + w)(\Phi')^2\right]$$
$$+6\mathcal{H}(1+w)\partial_i\Phi'\partial_j\Phi'\left[(1 + c_s^2)(12\mathcal{H}^3\Phi^2 + \Phi'\partial^2\Phi - 4\mathcal{H}\Phi\partial^2\Phi - 3\mathcal{H}(\Phi')^2)\right.$$

$$+3\mathcal{H}^2(-1 + 3c_s^2 - 4w)\Phi\Phi'] - 3\mathcal{H}^3(1+w)\partial_i\Phi\partial_j\Phi\left[(1 + c_s^2)(2\Phi'\partial^2\Phi - 8\mathcal{H}\Phi\partial^2\Phi + 18\mathcal{H}^2\Phi\Phi')\right.$$
$$\left.\left. - 3\mathcal{H}(3 + 2c_s^2 + w)(\Phi')^2 + 6\mathcal{H}^3(11 + 4c_s^2 + 22w + 15w^2)\Phi^2\right]\right\}$$

(Equation 54)

Setting $w = c_s^2 = 1/3$ during RD, they return to the source terms used in Yuan et al. (2019a). In our convention, the density parameter for high-order corrections takes the same form as Equation (33). After defining the Fourier transform of S_{ij} to be

$$\mathcal{S}(\boldsymbol{k}, \eta) = -4e^{ij}S_{ij}(\boldsymbol{k}) = \mathcal{S}^{(2)}(\boldsymbol{k}, \eta) + \mathcal{S}^{(3)}(\boldsymbol{k}, \eta) + \mathcal{S}^{(4)}(\boldsymbol{k}, \eta),$$

(Equation 55)

then we can write the source terms as

$$\mathcal{S}^{(2)}(\boldsymbol{k}, \eta) = 4\int\frac{d^3p}{(2\pi)^{3/2}}\mathbf{e}_k(\boldsymbol{p}, \boldsymbol{p})F^{(2)}(p, |\boldsymbol{k}-\boldsymbol{p}|, \eta)\Phi_p\Phi_{|k-p|},$$

(Equation 56)

$$\mathcal{S}^{(3)}(\boldsymbol{k}, \eta) = 4\int\frac{d^3pd^3q}{(2\pi)^3}\mathbf{e}_k(\boldsymbol{p}, \boldsymbol{q})F^{(3)}(p, q, |\boldsymbol{k}-\boldsymbol{p}-\boldsymbol{q}|, \eta)\Phi_p\Phi_q\Phi_{|k-p-q|},$$

(Equation 57)

$$\mathcal{S}^{(4)}(\boldsymbol{k}, \eta) = 4\int\frac{d^3pd^3qd^3l}{(2\pi)^{9/2}}\left[\mathbf{e}_k(\boldsymbol{l}, \boldsymbol{l})F_1^{(4)}(p, q, l, |\boldsymbol{k}-\boldsymbol{p}-\boldsymbol{q}-\boldsymbol{l}|, \eta)\right.$$

(Equation 59)

$$\left. + \mathbf{e}_k(\boldsymbol{p}, \boldsymbol{q})F_2^{(4)}(p, q, l, |\boldsymbol{k}-\boldsymbol{p}-\boldsymbol{q}-\boldsymbol{l}|, \eta)\right]\Phi_p\Phi_q\Phi_l\Phi_{|k-p-q-l|},$$

where we have defined $\mathbf{e}_k(\boldsymbol{p}, \boldsymbol{q}) \equiv e^{ij}(\boldsymbol{k})p_iq_j$. The contribution for the cross mode is omitted here since the plus mode, and cross mode have the same energy density and we can sum over the polarization mode at the final step. In Equation (56), the time evolution of Φ is absorbed in the transfer function, namely

$$F^{(2)}(\boldsymbol{q}_1, \boldsymbol{q}_2, \eta) = \frac{1}{\mathcal{H}^2}\left(3\mathcal{H}^2 T_{q_1} T_{q_2} + \mathcal{H}(T_{q_1} T'_{q_2} + T'_{q_1} T_{q_2}) + T'_{q_1} T'_{q_2}\right),$$

$$F^{(3)}(\boldsymbol{q}_1, \boldsymbol{q}_2, \boldsymbol{q}_3, \eta) = \frac{1}{3\mathcal{H}^4}\Big\{2\mathcal{H}^2 T_{q_1} T_{q_2}\left[(18\mathcal{H}^2 - q_3^2)T_{q_3} - 6\mathcal{H}T_{q_3}'\right] - 2T_{q_1}'T_{q_2}'\left[(6\mathcal{H}^2 + q_3^2)T_{q_3} + 3\mathcal{H}T_{q_3}'\right]$$

$$-\mathcal{H}\left(T_{q_1}T_{q_2}' + T_{q_1}'T_{q_2}\right)\left(2q_3^2 T_{q_3} + 9\mathcal{H}T_{q_3}'\right)\Big\}$$

$$F_1^{(4)}(\boldsymbol{q}_1, \boldsymbol{q}_2, \boldsymbol{q}_3, \boldsymbol{q}_4, \eta) = 16\, T_{q_1} T_{q_2} T_{q_3} T_{q_4},$$

$$F_2^{(4)}(\boldsymbol{q}_1, \boldsymbol{q}_2, \boldsymbol{q}_3, \boldsymbol{q}_4, \eta) = \frac{1}{36\mathcal{H}^6}\Big\{\mathcal{H}^2 T_{q_1} T_{q_2}\Big[-108\mathcal{H}^2 T'_{q_3} T'_{q_4} + 48\mathcal{H}^2(24\mathcal{H}^2 + q_3^2 + q_4^2)T_{q_3} T_{q_4}$$

$$+ 12\mathcal{H}(9\mathcal{H}^2 - q_3^2)T_{q_3} T'_{q_4} + 12\mathcal{H}(9\mathcal{H}^2 - q_4^2)T'_{q_3} T_{q_4}\Big]$$

$$+ T'_{q_1} T'_{q_2}\Big[72\mathcal{H}^2 T'_{q_3} T'_{q_4} - 48\mathcal{H}^2(6\mathcal{H}^2 + q_3^2 + q_4^2)T_{q_3} T_{q_4}$$

$$+ 12\mathcal{H}(3\mathcal{H}^2 + q_3^2)T_{q_3} T'_{q_4} + 12\mathcal{H}(3\mathcal{H}^2 + q_4^2)T'_{q_3} T_{q_4}\Big]$$

$$-\left(\mathcal{H}T_{q_1} + T'_{q_1}\right)\left(\mathcal{H}T_{q_2} + T'_{q_2}\right)\Big[12\mathcal{H}(21\mathcal{H}^2 + 5q_3^2)T_{q_3} T'_{q_4}$$

$$+ 12\mathcal{H}(21\mathcal{H}^2 + 5q_4^2)T'_{q_3} T_{q_4} + 180\mathcal{H}^2 T'_{q_3} T'_{q_4}$$

$$+ 8(18\mathcal{H}^4 + 9\mathcal{H}^2 q_3^2 + 9\mathcal{H}^2 q_4^2 + 2q_3^2 q_4^2)T_{q_3} T_{q_4}$$

$$+ 3\boldsymbol{q}_3 \cdot \boldsymbol{q}_4\left(11\mathcal{H}^2 T_{q_3} T_{q_4} - \mathcal{H}T_{q_3} T'_{q_4} - \mathcal{H}T'_{q_3} T_{q_4} - T'_{q_3} T'_{q_4}\right)\Big]\Big\}$$

(Equation 60)

where we set $w = c_s^2 = 1/3$. The notation T_k is short for the time evolution function, $T_\Phi(k\eta)$. Applying the Green's function method, the solution to $h_{ij}^{(n)}$ takes the same form as Equation (29). The next-order corrections to Ω_{GW} comes from two parts. The first part is the coupling of $S_{ij}^{(3)}$ itself,

$$\Omega_{GW}^i(k, \eta) = \frac{k^3}{384\pi^2}\left(\frac{k}{\mathcal{H}}\right)^2 \int d\tilde{\eta}_1 \frac{a(\tilde{\eta}_1)}{a(\eta)} g_k(\eta; \tilde{\eta}_1) \int \tilde{\eta}_2 \frac{a(\tilde{\eta}_2)}{a(\eta)} g_k(\eta, \tilde{\eta}_2) \int d^3p\, d^3q \frac{P_\Phi(|\boldsymbol{p} - \boldsymbol{q}|)}{|\boldsymbol{p} - \boldsymbol{q}|^3} \frac{P_\Phi(q)}{q^3} \frac{P_\Phi(|\boldsymbol{k} - \boldsymbol{p}|)}{|\boldsymbol{k} - \boldsymbol{p}|^3}$$

$$\times \Big[2e_k(\boldsymbol{p} - \boldsymbol{q}, \boldsymbol{q})^2 F^{(3)}\left(q, |\boldsymbol{p} - \boldsymbol{q}|, |\boldsymbol{k} - \boldsymbol{p}|, \tilde{\eta}_1\right) F^{(3)}\left(q, |\boldsymbol{p} - \boldsymbol{q}|, |\boldsymbol{k} - \boldsymbol{p}|, \tilde{\eta}_2\right)$$

$$+ 4e_k(\boldsymbol{p}, \boldsymbol{p} - \boldsymbol{q})e_k(\boldsymbol{p}, \boldsymbol{q}) F^{(3)}\left(|\boldsymbol{k} - \boldsymbol{p}|, |\boldsymbol{p} - \boldsymbol{q}|, q, \tilde{\eta}_1\right) F^{(3)}\left(q, |\boldsymbol{k} - \boldsymbol{p}|, |\boldsymbol{p} - \boldsymbol{q}|, \tilde{\eta}_2\right)\Big],$$

(Equation 61)

while the second part is the coupling of $S_{ij}^{(2)}$ and $S_{ij}^{(4)}$

$$\Omega_{GW}^{ii}(k, \eta) = \frac{k^3}{384\pi^2}\left(\frac{k}{\mathcal{H}}\right)^2 \int d\tilde{\eta}_1 \frac{a(\tilde{\eta}_1)}{a(\eta)} g_k(\eta; \tilde{\eta}_1) \int \tilde{\eta}_2 \frac{a(\tilde{\eta}_2)}{a(\eta)} g_k(\eta, \tilde{\eta}_2) \int d^3p\, d^3q \frac{P_\Phi(p)}{p^3} \frac{P_\Phi(q)}{q^3} \frac{P_\Phi(|\boldsymbol{k} - \boldsymbol{p}|)}{|\boldsymbol{k} - \boldsymbol{p}|^3}$$

$$\times e_k(\boldsymbol{p}, \boldsymbol{p}) F^{(2)}\left(\boldsymbol{p}, \boldsymbol{k} - \boldsymbol{p}, \tilde{\eta}_1\right)\Big\{6\Big[e_k(\boldsymbol{p}, \boldsymbol{p}) + e_k(\boldsymbol{q}, \boldsymbol{q})\Big]F_1^{(4)}\left(\boldsymbol{p}, \boldsymbol{k} - \boldsymbol{p}, \boldsymbol{q}, \boldsymbol{q}, \tilde{\eta}_2\right)$$

$$- 2e_k(\boldsymbol{p}, \boldsymbol{p})F_2^{(4)}\left(\boldsymbol{p}, \boldsymbol{k} - \boldsymbol{p}, \boldsymbol{q}, -\boldsymbol{q}, \tilde{\eta}_2\right) - 8e_k(\boldsymbol{p}, \boldsymbol{q})F_2^{(4)}\left(\boldsymbol{p}, \boldsymbol{q}, \boldsymbol{q}, \boldsymbol{k} - \boldsymbol{p}, \tilde{\eta}_2\right)$$

$$- 2e_k(\boldsymbol{q}, \boldsymbol{q})F_2^{(4)}\left(\boldsymbol{q}, \boldsymbol{q}, \boldsymbol{p}, \boldsymbol{k} - \boldsymbol{p}, \tilde{\eta}_2\right)\Big\}$$

(Equation 62)

The next-order corrections of Ω_{GW} is the sum of Equation (61) and Equation (62). For a δ-spectrum, these two expressions can be further simplified after integrate over the δ function (see Yuan et al. (2019a) for results). After considering the higher-order corrections, the deep valley at $k=2/3k_*$ generated at second-order will be smoothed to a finite value. Moreover, the cutoff frequency will be extended from $2k_*$ to $3k_*$. See Figure 4.

The above calculation only focus on the GWs induced by the linear-order scalar perturbations. However, the higher-order scalar, vector and tensor perturbations will contribute to the higher-order SIGWs. Recently, the SIGWs induced by the second-order perturbations were analytically studied in Zhou et al. (2021). But the complete calculation of the next-order correction to SIGWs has not been explored yet.

SIGWs within non-gaussianities

GWs generated by non-Gaussian scalar perturbations were first estimated by Nakama et al. (2017) where they found that the amplitude of SIGWs could be suppressed by non-Gaussianities to several orders of magnitude. After Espinosa et al. (2018); Kohri and Terada (2018a) proposed the semi-analytical method to calculate SIGWs, Cai et al. (2019a); Unal (2019) calculate the non-Gaussian effects on SIGWs by considering a local-type non-Gaussianities up to second-order (or F_{NL}-order). They both argued that SIGWs within non-Gaussianities have observable signatures which can be used to probe primordial non-Gaussianities. However, in a more recent study Yuan and Huang (2020), Yuan et al. revisited the non-Gaussian effects and extended the calculation to third-order (or G_{NL}-order non-Gaussianities). They argue that all the non-Gaussian effects are degenerate with the power spectrum. Hence it is impossible to read any information about non-Gaussianities only through the signal of SIGWs.

To see this more clear, let us go back to the first line of Equation (34), where one needs to compute the two-point correlator of the source terms. This will lead to the four-point correlator of Φ, namely $\langle \Phi_p \Phi_{k-p} \Phi_q \Phi_{k'-q} \rangle$. If Φ obeys Gaussian distribution, then the four-point correlator can be simplified to three two-point correlators through Wick's theorem. However, the general formula for the four-point correlator is

$$\langle \Phi_p \Phi_{k-p} \Phi_q \Phi_{k'-q} \rangle = \langle \Phi_p \Phi_{k-p} \Phi_q \Phi_{k'-q} \rangle_c + \langle \Phi_p \Phi_{k-p} \rangle \langle \Phi_q \Phi_{k-q} \rangle + \langle \Phi_p \Phi_q \rangle \langle \Phi_{k-p} \Phi_{k'-q} \rangle + \langle \Phi_p \Phi_{k'-q} \rangle \langle \Phi_{k-p} \Phi_q \rangle$$

(Equation 63)

where we assume that $\langle \Phi \rangle = 0$ and $\langle \Phi_p \Phi_{k-p} \Phi_q \Phi_{k'-q} \rangle_c$ is the connected four-point correlation function (4PCF) (or called the fourth cumulant in statistics) which is related to the trispectrum, $\mathcal{T}_\Phi$, by

$$\langle \Phi_p \Phi_{k-p} \Phi_q \Phi_{k'-q} \rangle_c = (2\pi)^3 \delta(k + k') \mathcal{T}_\Phi(p, q, k, k').$$

(Equation 64)

The connected 4PCF will vanish if Φ is a Gaussian variable. Otherwise it will contribute to be SIGWs Unal (2019). In Unal (2019); Cai et al. (2019a), the authors consider a local-type non-Gaussianities up to F_{NL}-order and calculate the SIGWs in the absence of the connected 4PCF. After that, the G_{NL}-order is studied by Yuan and Huang (2020) still in the absence of the connected 4PCF. Recently, Atal and Domènech (2021) considered the leading order of the connected 4PCF and Adshead et al. (2021) included the complete contribution of the connected 4PCF. Although non-Gausiannities can alter the waveform of the SIGW signal, one cannot read any information about non-Gaussianities only through the signal of $\Omega_{GW}(f)$. This is because the non-Gaussian effects are absorbed into the total 4PCF and there will be a degeneracy between the non-Gaussian effects and the total 4PCF. Therefore, one cannot tell from the total 4PCF whether there is an evidence for non-Gaussianities (or for the connected 4PCF).

Gauge issue of SIGWs

Although the tensor mode are gauge invariant at first-order, they fail to remain gauge invariant at second-order (see, e.g., Noh and Hwang (2003)). Therefore, a natural question arises: Is the energy density of SIGWs gauge dependent or not?

For a long time, Newton gauge has been a commonly used gauge to compute SIGWs since the degrees of freedom are fixed completely in this gauge, and there is no residual gauge freedom. In Newton gauge, the scalar mode φ is the just Bardeen potential Φ and all the degrees of freedom are fixed, which make Newton gauge the most mathematically convenient gauge for evaluating SIGWs. SIGWs in other gauges were first calculated numerically by Hwang et al. Hwang et al. (2017) where they investigated Ω_{GW} in uniform expansion gauge, comoving gauge and uniform curvature gauge and they found that Ω_{GW} is gauge dependent. After that, the semi-analytical method was developed, and Gong calculated the SIGWs in comoving gauge during MD Gong (2019). Gong's result showed that h_{ij} increases as η^2 in comoving gauge. Another study by Tomikawa and Kobayashi appeared at the same time Tomikawa and Kobayashi (2019), where they investigate the SIGWs in comoving gauge and uniform curvature gauge. They found that the results in comoving gauge increase with time for $w \geq 0$ while the result in uniform curvature gauge is identical with that in

Newton gauge for $w > 0$. Moreover, they found that the results are all different in Newton gauge, comoving gauge, and uniform curvature gauge if $w = 0$.

Owing to the gauge dependence of Ω_{GW}, it is natural to ask which gauge is relevant in interpreting the observations. This question is discussed by De Luca et al. De Luca et al. (2019a). They calculated the SIGWs in synchronous gauge since they argued that the sensitivity curves of LISA are given in that gauge. By neglecting the E mode but keeping its derivatives in the source term, De Luca et al. found that the SIGWs in synchronous gauge are identical to that of Newton gauge. Their results are later confirmed by Yuan et al. (2019c); Inomata and Terada (2019). However, the calculation of SIGWs in synchronous gauge is an a tough nut since there is residual gauge freedom in E mode. The complete calculation in synchronous gauge and which gauge is relevant for observations are still open questions.

In synchronous gauge, $\delta g_{00} = \delta g_{0i} = 0$, corresponding to $\tilde{\varphi} = \tilde{B} = 0$ in Equation (19). This leads to Lu et al. (2020).

$$T^S(\eta) = -\frac{1}{a}\left(\int_0^\eta a(\tilde{\eta})\varphi(\tilde{\eta})\mathrm{d}\tilde{\eta} - \mathcal{C}_1(\boldsymbol{x})\right) \qquad \text{(Equation 65)}$$

$$L^S(\eta) = \int_0^\eta\left[T^S(\tilde{\eta}) - B(\tilde{\eta})\right]\mathrm{d}\tilde{\eta} + \mathcal{C}_2(\boldsymbol{x}), \qquad \text{(Equation 66)}$$

where $\mathcal{C}_1$ and $\mathcal{C}_2$ are two arbitrary spatial functions. The presence of $\mathcal{C}_1$ and $\mathcal{C}_2$ come from the residual gauge freedom in synchronous gauge. To determine the time slicing and the spatial coordinate on the hypersurface, one has to fix $\mathcal{C}_1$ and $\mathcal{C}_2$. To see the impacts of residual gauge freedom more clearly, we derive the equation of motion for the scalar modes during RD, namely

$$2\mathcal{H}E' + E'' + \psi = 0, \qquad \text{(Equation 67)}$$
$$6\psi'' + 2\mathcal{H}(9\psi' - 4\partial^2 E) - 3\partial^2 E'' - 5\partial^2\psi = 0. \qquad \text{(Equation 68)}$$

After some algebra, one can get the equation of motion for E, (see also Lu et al. (2020))

$$x^3 T_E''''(x) + 5x^2 T_E'''(x) + \left(2 + \frac{x^2}{3}\right)x T_E''(x) - \left(2 - \frac{x^2}{3}\right)T_E'(x) = 0, \qquad \text{(Equation 69)}$$

where the transfer function for E and ψ are defined as

$$k^2 E(\boldsymbol{k}) \equiv \Phi_k T_E(k\eta) \qquad \text{(Equation 70)}$$
$$\psi(\boldsymbol{k}) \equiv \Phi_k T_\psi(k\eta). \qquad \text{(Equation 71)}$$

In our convention, the boundary condition for the transfer function should be $T_\psi(x \to 0) = 3/2$ in order to match the relation between curvature perturbation and the Bardeen potential. The general solution for Equation (69) is

$$T_E(x) = \mathcal{C}_3 + \mathcal{C}_4\left(\mathrm{Ci}(z) - \frac{\sin(z)}{z}\right) + \mathcal{C}_5\ln(z) + \mathcal{C}_6\left(\mathrm{Si}(z) + \frac{\cos(z)}{z}\right), \qquad \text{(Equation 72)}$$

where $z \equiv x/\sqrt{3}$ and $\mathcal{C}_i, (i = 3, 4, 5, 6)$ are integrate constants. One can check that under the residual gauge transformation,

$$T = -\frac{\mathcal{C}_7}{x} \qquad \text{(Equation 73)}$$
$$L = -\mathcal{C}_7\ln x + \mathcal{C}_8, \qquad \text{(Equation 74)}$$

the gauge condition $\tilde{\varphi} = \tilde{B} = 0$ still satisfy. Combining Equation (72) and Equation (74), we see that $\mathcal{C}_8$ can be absorbed by $\mathcal{C}_3$ while $\mathcal{C}_7$ corresponds to $\mathcal{C}_5$. In other words, the constant $\mathcal{C}_3$ and the logarithm term are two independent pure gauge modes. One can arbitrarily choose $\mathcal{C}_3$ and $\mathcal{C}_5$ to work in a specific hypersurface. After selecting the hypersurface, the solution can be well determined after performing the only physical condition, $T_\psi(x \to 0) = 3/2$. Here comes a big problem in synchronous gauge. The solution to E mode will definitely diverge either at the initial time or at a late time. For instance, let's assume that $T_E(x)$ have a finite value at $x = 0$. Notice that the Taylor expansion of cosine integral function at $x = 0$ is $\mathrm{Ci}(x) = \gamma + \ln(x) + \mathcal{O}(x^2)$, where γ is the Euler gamma constant. Therefore, one must choose $\mathcal{C}_5 = -\mathcal{C}_4$ so that the logarithm term can be canceled by the $\mathrm{Ci}(x)$ term. By applying the boundary condition $T_\psi(0) = 3/2$, one gets $\mathcal{C}_6 = 0$ and $\mathcal{C}_4 = -\mathcal{C}_5 = 9$ and the finite value at $x = 0$ is given by $T_E(0) = \mathcal{C}_3 + 9\gamma$. However, under this situation, we see that the $T_E(x)$ at a late time will diverge according to the logarithm term in Equation (72). The

consequence of the divergence is that the *E* mode will induce the GWs continuously during RD, resulting in the divergence of Ω_{GW} for SIGWs. On the other hand, if we let the gauge mode $\mathcal{C}_5$ vanish, the presence of the Ci(*x*) term will result in the divergence at the initial time. A physical interpretation is that if the observer requires a converged initial condition, the geodesics of the observer using as a reference may collapse or cross each other. So one has to change the residual gauge freedom to adjust the reference system. This makes the calculation of SIGWs in synchronous gauge very complicated.

In De Luca et al. (2019a); Yuan et al. (2019c); Inomata and Terada (2019), the authors calculated the SIGWs in the absence of *E* mode but considering its derivatives where the gauge freedom are completely fixed. In this situation, the energy density of SIGWs agrees with that in Newton gauge. Moreover, it was shown in Lu et al. (2020) that if throwing away the pure gauge modes, the result returns to that in Newton gauge. These studies indicate that the large divergence of SIGWs in synchronous gauge comes from the residual gauge freedom and the synchronous gauge seems to be ill-defined for calculating the SIGWs. Readers interested in the calculation of different gauge can refer to Lu et al. (2020); Ali et al. (2020); Inomata (2020).

Since the standard procedure to calculate the energy density of h_{ij} brings divergence, one way to tackle the problem is to find a new gauge invariant quantity for the GWs. One can construct infinite gauge invariant variables for scalar and tensor perturbations. However, the point is to find a quantity that can interpret the physical world and the measurements. This idea has been tried by Zhang, Wang and Zhu in Chang et al. (2020a, 2020b). By applying the technique of Lie derivative, they constructed gauge invariant second-order GWs in synchronous gauge, which is related to the measurement, and their results coincide with that computed in Newton gauge. They also used this idea to evaluate the energy density of SIGWs in uniform density gauge, which is supposed to diverge as η^6. They found the new gauge invariant second-order GWs converged and were identical with the one in Newton gauge Chang et al. (2020c). In a more recent study Domènech and Sasaki (2020), it is shown that the current Ω_{GW} is well defined in most of gauges if one takes the sub-horizon limit, namely $\eta \rightarrow \infty$. The authors found that Ω_{GW} will be the same as that in Newton gauge if the trace part of the metric perturbation at sub-horizon limit is the order of or smaller than the scalar perturbation Φ in Newton gauge (see Equation (3.2) or Equation (3.5) in Domènech and Sasaki (2020)). They also pointed out that, for particular choices of the residual gauge freedom, synchronous gauge can give the same result in Newton gauge.

Although the synchronous gauge is relevant for observations, Newton gauge is still the most popular gauge since it not only gives the same result as synchronous gauge but also is the simplest gauge to perform the calculation.

SEARCHING FOR PBH DM USING SIGWS

SIGWs provide the most efficient way so far to search for PBH DM. This is due to the fact that PBHs might from the peak of scalar perturbations, which is extremely sensitive to the amplitude of the power spectrum, *A*. Let's consider a monochromatic power spectrum for example, described by Equation (40). The variance of the perturbations generated by this spectrum is $\sigma = \int P_\zeta(k)\mathrm{d}\ln k = A$. Using the Press-Schechter formalism, Equation (11), the mass function can be approximated as

$$\beta = \frac{1}{2}\mathrm{erfc}\left(\frac{\nu_c}{\sqrt{2}}\right) = \sqrt{\frac{1}{2\pi}} \ \frac{e^{-\nu_c^2/2}}{\nu_c} \propto \sqrt{A} \ e^{-\frac{\Delta_c^2}{2A}}, \qquad \text{(Equation 75)}$$

which is exponentially dependent on *A*. On the other hand, the inevitably generated SIGWs satisfy $h_{ij} \propto A$. Therefore, a small change in *A* would change f_{pbh} by several orders of magnitude.

To further quantify the power of SIGWs, we shall estimate the expected signal-to-noise ratio (SNR) by the GW detector, which is evaluated as Allen and Romano (1999); Thrane and Romano (2013),

$$\rho^2 = T \int \mathrm{d}f \ \frac{\Gamma(f)^2 S_h(f)^2}{\left[\frac{1}{25} + \Gamma(f)^2\right] S_h(f)^2 + P_n(f)^2 + \frac{2}{5}S_h(f)P_n(f)}, \qquad \text{(Equation 76)}$$

The strain power spectral density is given by $S_h(f) = 3H_0^2\Omega_{\mathrm{GW},0}/(2\pi^2 f^3)$. $\Gamma(f)$ is the overlap function and $P_n(f)$ is the noise power spectral density. For LISA, $\Gamma(f) = R(f)$ where $R(f)$ is the signal transfer function of LISA and
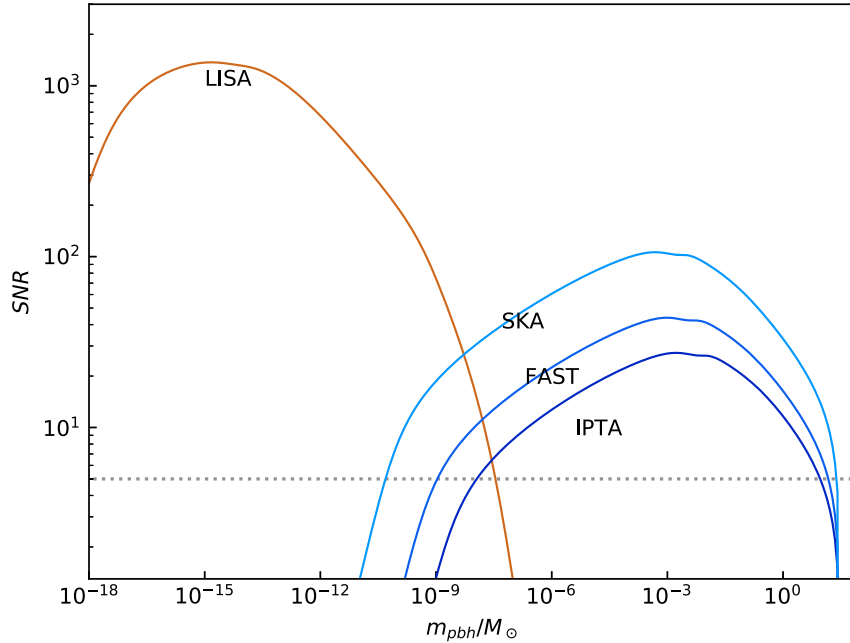
Figure 5. The expected SNR by LISA/IPTA/FAST/IPTA in detecting SIGWs generated by monochromatic PBHs
The dotted line corresponds to SNR=5. We assume the observation time to be $T = 4$yr for LISA and $T = 30$yr for PTAs. The value of Δt, N and σ for current PTAs can be found in Kuroda et al. (2015) (see Table 5).

its expression should be computed numerically Larson et al. (2000) but it can be well fit by Robson et al. (2019).

$$R(f) = \frac{3}{10\left(1 + 0.6(f/f_\star)^2\right)},$$ (Equation 77)

where $f_\star = c/(2\pi L) = 19.09$ mHz is the transfer frequency and $L = 2.5$ Gm for the current LISA design. On the other hand, $P_n(f)$ can be approximated by Robson et al. (2019).

$$P_n(f) = \frac{P_{\text{oms}}}{L^2} + 2\left(1 + \cos^2(f / f_\star)\right)\frac{P_{\text{acc}}}{(2\pi f)^4 L^2}.$$ (Equation 78)

The optical metrology noise spectrum and the acceleration noise is parameterized by Robson et al. (2019).

$$P_{\text{oms}}(f) = \left(1.5 \times 10^{-11}\text{m}\right)^2\left(1 + \left(\frac{2\text{mHz}}{f}\right)^4\right)\text{Hz}^{-1}$$ (Equation 79)

$$P_{\text{acc}}(f) = \left(3 \times 10^{-15} \text{ m s}^{-2}\right)^2\left(1 + \left(\frac{0.4\text{mHz}}{f}\right)^2\right)\left(1 + \left(\frac{f}{8\text{mHz}}\right)^4\right)\text{Hz}^{-1}.$$ (Equation 80)

For PTA, the expressions are $\Gamma(f) = R(f) = 1/(12\pi^2 f^2)$ and $P_n(f) = 2\Delta t\sigma^2$ where Δt is the observation time and σ is the root-mean-square timing noise. For PTAs, each of the millisecond pulsars can be regarded as a single GW detector, and one has to average the spatial contribution such that Allen and Romano (1999); Siemens et al. (2013).

$$\rho^2 = 2T \sum_{I,J}^{M} \zeta_{IJ}^2 \left[\int \text{d}f \frac{R(f)^2 S_h(f)^2}{\left[\frac{1}{25} + R(f)^2\right]S_h(f)^2 + P_n(f)^2 + \frac{2}{5}S_h(f)P_n(f)}\right],$$ (Equation 81)

where ζ_{IJ} is the normalized Hellings and Downs coefficient for pulsars I and J. Assuming the pulsars are distributed homogeneously on the sky, then ζ_{IJ} takes the form
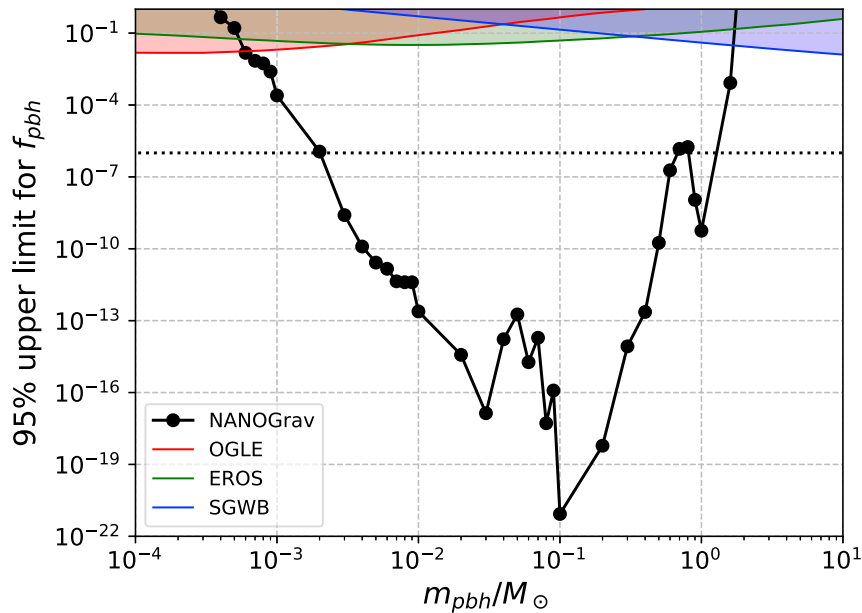
Figure 6. The constraints on f_{pbh} through the null detection of SIGWs by NANOGrav 11-yr observations
The dotted line corresponds to 10^{-6}. The colored region are the results excluded by OGLE microlensing Niikura et al. (2019b), EROS microlensing Tisserand et al., (2007) and the SGWB from PBH binaries Chen and Huang (2019). Taken from Figure 2 in Chen et al. (2019b).

$$\zeta_{IJ} = N(N-1)\frac{4.74}{20 \times 19}, \tag{Equation 82}$$

where N is the number of pulsars. Combing the above equations, we can estimate the expected SNR from monochromatic PBHs and scan the mass of PBHs. The result is shown in Figure 5. PBHs lighter than $\lesssim 10^{-18} M_\odot$ have already evaporated through Hawking radiation by today and is not shown in the figure.

If the PTAs and LISA fail to detect the SIGWs from PBHs, an upper limit can be placed for f_{pbh}. In Wang et al. (2019b), Wang et al. found the constraints on f_{pbh} can reach 10^{-13} for $m_{pbh} \in [10^{-8}, 1]M_\odot$. Chen et al. Chen et al. (2019b) searched the SIGW signals in the NANOGrav 11-yr data set for monochromatic PBHs. They scan the mass of PBHs and did not find the SIGW signal. Therefore they placed an upper limit on f_{pbh}, see Figure 6. As shown in the figure, the constraints from SIGW are several orders of magnitude better than the other constraints. Recently, NANOGrav has reported strong evidence for a common-spectrum process modeled as power-law in the 12.5-year data set. Various models have been put forward to explain the signal assumed to be gravitational waves. SIGWs generated by a broad and flat power spectrum seems to give one possible explanation De Luca et al. (2021); Sugiyama et al. (2021) among the various cosmological and astrophysical models. See also Vaskonen and Veermäe (2021); Kohri and Terada (2021); Domènech and Pi (2020); Inomata et al. (2020d). However, further analysis indicates that the signal is preferred to be scalar transverse modes in the general metric theory rather than the gravitational waves predicted in general relativity Chen et al. (2021).

Another study was carried out by Kapadia et al. Kapadia et al. (2020b) where they explored the SIGW signal in the LIGO data. Kapadia et al. reported a null detection of SIGW signal and thus placing a severe constraint on f_{pbh} to be less than a few parts in million. Their work provides another independent test in addition to the γ-ray burst Carr et al. (2010) in this mass window.

Up to now there are various independent cosmological observations constraining the fraction of PBHs in Figure 7. For $m_{pbh} \lesssim 10^{-18} M_\odot$, PBHs are severely constrained through the null detections of extra-galactic Gamma-ray background (EGB) from PBH evaporation Carr et al. (2010). On the other hand, PBHs heavier than $\sim 10^3 M_\odot$ are tightly constrained by the CMB observations through the accreting PBHs Ali-Haimoud and Kamionkowski (2017); Aloni et al. (2017); Horowitz (2016); Chen et al. (2016). In the mass range
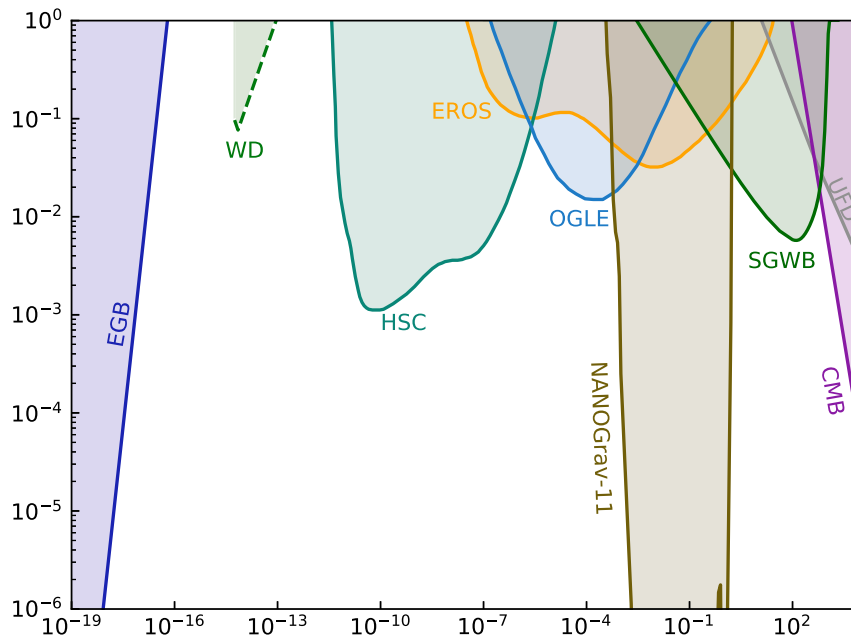
Figure 7. An overview on the current observational constraints on f_{pbh}

Constraints are taken from EGB Carr et al. (2010), WDs Graham et al. (2015), HSC Niikura et al. (2019a), EROS Tisserand et al., (2007), OGLE Niikura et al. (2019b), SGWB from binary PBHs Wang et al. (2018); Chen and Huang (2019), UFD Brandt (2016), and SIGWs using NANOGrav 11-yr data set Chen et al. (2019b).

$m_{pbh} \in [10^{-18}, 10^3]M_\odot$, f_{pbh} are constrained to no more than a few in thousand by numerous astrophysical observations. For example, microlensing events such as Subaru/HSC Niikura et al. (2019a), Kepler Griest et al. (2013), OGLE Niikura et al. (2019b), and EROS/MACHO Tisserand et al., (2007) and the dynamical heating of ultra-faint dwarf galaxies Brandt (2016). On the other hand, GWs physics also placed broad constraints on f_{pbh}, such as the merger events from binary PBHs in the subsolar mass range Abbott et al., (2018); Magee et al. (2018); Chen and Huang (2019); Abbott et al. (2019) and the null detections of stochastic GW background (SGWB) from binary PBHs with LIGO Wang et al. (2018); Chen and Huang (2019). Although the existence of white dwarfs (WDs) in our local galaxy have also placed constraints on f_{pbh} Graham et al. (2015). However, this constraint has been challenged by a recent paper Montero-Camacho et al. (2019), and we label the constraint from WDs with the dashed line in Figure 7. Despite the above constraints, PBHs in a substantial window $\sim [10^{-16}, 10^{-14}] \cup [10^{-13}, 10^{-12}]M_\odot$ are still allowed to account for all of the DM.

Although SIGWs place the currently severest constraint on f_{pbh}, it is based on the standard PBH formation model in which PBHs are formed from the critical collapse of overdensity. However, other mechanism of the PBH formation has been proposed (see e.g., Cotner et al. (2019)), and the constraints from SIGWs are not valid for those PBHs.

SUMMARY AND OUTLOOK

PBHs can represent the DM in our Universe and explain the merger events detected by LIGO/VIRGO if $f_{pbh} \sim 10^{-3}$ in that mass range. We focus on the standard PBH formation model, where the PBHs are formed through the collapse of the overdensity in the very early Universe. We have review several aspects of PBH formation, and the SIGWs produced from PBHs studied over the past decades.

First of all, we review the calculation of the PBH formation. The formation of PBHs depends on the power spectrum of the scalar perturbations, the window function, the primordial non-Gaussianities, intrinsic non-Gaussianities, and the critical value beyond which PBH can form.

Secondly, we consider the SIGWs inevitably generated during the formation of PBHs. We review the relevant works concerning SIGWs over the past decades. SIGW is a solid prediction of general relativity. But due to the unknown of primordial scalar power spectrum on small scales, the waveform of the SIGW background is

model-dependent which make the detection of SIGWs very difficult. Fortunately, the logarithm scaling in the infrared region is a model-independent feature for SIGWs, making SIGWs unique from other SGWB. We also review the impacts from the cosmological background, higher-order corrections to SIGWs, primordial non-Gaussianities. Finally, we discuss the gauge issues of SIGWs. On the other hand, the presence of primordial non-Gaussianities is an essential aspect since it could dramatic change the waveform and the amplitude of the SIGWs. For local-type non-Gaussianities, as long as monochromatic PBH in the allowing mass window represents all the DM, then LISA and PTAs should detect the signals irrespective of F_{NL}. However, up to G_{NL}-order, this conclusion no longer holds. The G_{NL}-order could further suppress the SIGWs than F_{NL}-order and thus avoiding the detection of LISA. Another important impact of non-Gaussianities is that the power spectrum and the non-Gaussianities are degenerate. As a result, one cannot tell the presence of non-Gaussianities only through the SIGW signal unless considering another independent observation.

So far, SIGW has placed the most severe constraint on f_{pbh} Chen et al. (2019b). However, this results from monochromatic PBHs in the absence of primordial non-Gaussianities and neglecting the QCD phase transition. During the QCD epoch, the equation of state and the sound speed decrease slightly from 1/ 3, thus changing the waveform of SIGWs. This will affect the PBHs within the PTA frequency band. Searching the SIGW signal for realistic models such as considering the QCD phase transition, a specific inflation model, and its loop correction to the power spectrum is necessary in this field.

Over the past decade, SIGWs from PBH DM have been widely studied. SIGW provides a promising tool to verify or falsify the PBH DM hypothesis. We are expected to witness intriguing progress in the coming decades.

ACKNOWLEDGMENTS

DECLARATION OF INTERESTS

The authors declare no competing interests.

REFERENCES

Abbott, B.P., Abbott, R., Abbott, T.D., braham, S.A., Acernese, F., Ackley, K., Adams, C., Adhikari, R.X., Adya, V.B., Affeldt, C., et al. (2019). LIGO Scientific, Virgo. arXiv:1904.08976 [astro-ph.CO].

Abbott, B.P., Abbott, R., Abbott, T.D., Abernathy, M.R., Acernese, F., Ackley, K., Adams, C., Adams, T., Addesso, P., Adhikari, R.X., et al. (2016). LIGO scientific, virgo). Phys. Rev. Lett. 116, 061102. arXiv:1602.03837 [gr-qc].

Abbott, B.P., Abbott, R., Abbott, T.D., Acernese, F., Ackley, K., Adams, C., Adams, T., Addesso, P., Adhikari, R.X., Adya, V.B., et al. (2018). LIGO scientific, virgo). Phys. Rev. Lett. 121, 231103. arXiv:1808.04771 [astro-ph.CO].

Abe, K.T., Tada, Y., and Ueda, I. (2020). arXiv:2010.06193 [astro-ph.CO].

Adshead, P., Lozanov, K.D., and Weiner, Z.J. (2021). arXiv:2105.01659 [astro-ph.CO].

Alabidi, L., Kohri, K., Sasaki, M., and Sendouda, Y. (2013). J. Cosmol. Astropart. Phys. 05, 033. arXiv:1303.4519 [astro-ph.CO].

Aldabergenov, Y., Addazi, A., and Ketov, S.V. (2021). Testing primordial black holes as dark matter in supergravity from gravitational waves. Phys. Lett. B 814, 136069. arXiv:2008.10476 [hep-th].

Ali, A., Gong, Y., and Lu, Y. (2020). arXiv:2009.11081 [gr-qc].

Ali-Haimoud, Y., and Kamionkowski, M. (2017). Phys. Rev. D95, 043534. arXiv:1612.05644 [astro-ph.CO].

Allen, B., and Romano, J.D. (1999). Phys. Rev. D 59, 102001. arXiv:gr-qc/9710117.

Aloni, D., Blum, K., and Flauger, R. (2017). J. Cosmol. Astropart. Phys. 1705, 017. arXiv:1612.06811 [astro-ph.CO].

Ananda, K.N., Clarkson, C., and Wands, D. (2007). Phys. Rev. D75, 123518. arXiv:gr-qc/0612013 [gr-qc].

Ando, K., Inomata, K., and Kawasaki, M. (2018a). Phys. Rev. D 97, 103528. arXiv:1802.06393 [astro-ph.CO].

Ando, K., Inomata, K., Kawasaki, M., Mukaida, K., and Yanagida, T.T. (2018b). Phys. Rev. D97, 123512. arXiv:1711.08956 [astro-ph.CO].

Ando, K., Kawasaki, M., and Nakatsuka, H. (2018c). Phys. Rev. D 98, 083508. arXiv:1805.07757 [astro-ph.CO].

Arroja, F., Assadullahi, H., Koyama, K., and Wands, D. (2009). Phys. Rev. D 80, 123526. arXiv:0907.3618 [astro-ph.CO].

Assadullahi, H., and Wands, D. (2010). Phys. Rev. D 81, 023527. arXiv:0907.4073 [astro-ph.CO].

Atal, V., and Domènech, G. (2021). arXiv:2103.01056 [astro-ph.CO].

Ballesteros, G., Rey, J., Taoso, M., and Urbano, A. (2020). Primordial black holes as dark matter and gravitational waves from single-field polynomial inflation. J. Cosmol. Astropart. Phys. 2020, 025. arXiv:2001.08220 [astro-ph.CO].

Bardeen, J.M., Bond, J.R., Kaiser, N., and Szalay, A.S. (1986). The statistics of peaks of Gaussian random fields. Astrophys. J. 304, 15.

Barnacka, A., Glicenstein, J.F., and Moderski, R. (2012). Phys. Rev. *D86*, 043001. arXiv:1204.2056 [astro-ph.CO].

Bartolo, N., De Luca, V., Franciolini, G., Lewis, A., Peloso, M., and Riotto, A. (2019a). Phys. Rev. Lett. *122*, 211301. arXiv:1810.12218 [astro-ph.CO].

Bartolo, N., De Luca, V., Franciolini, G., Peloso, M., Racco, D., and Riotto, A. (2019b). Phys. Rev. *D99*, 103521. arXiv:1810.12224 [astro-ph.CO].

Bartolo, N., Bertacca, D., De Luca, V., Franciolini, G., Matarrese, S., Peloso, M., Ricciardone, A., Riotto, A., and Tasinato, G. (2020). J. Cosmol. Astropart. Phys. *02*, 028. arXiv:1909.12619 [astro-ph.CO].

Baumann, D., Steinhardt, P.J., Takahashi, K., and Ichiki, K. (2007). Phys. Rev. D *76*, 084019. arXiv:hep-th/0703290 [hep-th].

Bhagwat, S., De Luca, V., Franciolini, G., Pani, P., and Riotto, A. (2021). J. Cosmol. Astropart. Phys. *01*, 037. arXiv:2008.12320 [astro-ph.CO].

Bhaumik, N., and Jain, R.K. (2020). arXiv:2009.10424 [astro-ph.CO].

Braglia, M., Hazra, D.K., Finelli, F., Smoot, G.F., Sriramkumar, L., and Starobinsky, A.A. (2020a). J. Cosmol. Astropart. Phys. *08*, 001. arXiv:2005.02895 [astro-ph.CO].

Braglia, M., Chen, X., and Hazra, D.K. (2020b). arXiv:2012.05821 [astro-ph.CO].

Brandt, T.D. (2016). Constraints on macho dark matter from compact stellar systems in ultra-faint dwarf galaxies. Astrophys. J. *824*, L31. arXiv:1605.03665 [astro-ph.GA].

Bugaev, E.V., and Klimai, P.A. (2010a). Bound on induced gravitational wave background from primordial black holes. JETP Lett. *91*, 1. arXiv:0911.0611 [astro-ph.CO].

Bugaev, E., and Klimai, P. (2010b). Phys. Rev. D *81*, 023517. arXiv:0908.0664 [astro-ph.CO].

Bugaev, E., and Klimai, P. (2011). Phys. Rev. D *83*, 083521. arXiv:1012.4697 [astro-ph.CO].

Bullock, J.S., and Primack, J.R. (1997). Non-Gaussian fluctuations and primordial black holes from inflation. Phys. Rev. D *55*, 7423. arXiv:astro-ph/9611106 [astro-ph].

Byrnes, C.T., Copeland, E.J., and Green, A.M. (2012). Phys. Rev. D *86*, 043512. arXiv:1206.4188 [astro-ph.CO].

Byrnes, C.T., Hindmarsh, M., Young, S., and Hawkins, M.R.S. (2018). J. Cosmol. Astropart. Phys. *08*, 041. arXiv:1801.06138 [astro-ph.CO].

Byrnes, C.T., Cole, P.S., and Patil, S.P. (2019). Steepest growth of the power spectrum and primordial black holes. J. Cosmol. Astropart. Phys. *06*, 028. arXiv:1811.11158 [astro-ph.CO].

Cai, R.-g., Pi, S., and Sasaki, M. (2019a). Phys. Rev. Lett. *122*, 201101. arXiv:1810.11000 [astro-ph.CO].

Cai, R.-G., Pi, S., Wang, S.-J., and Yang, X.-Y. (2019b). J. Cosmol. Astropart. Phys. *1905*, 013. arXiv:1901.10152 [astro-ph.CO].

Cai, R.-G., Pi, S., Wang, S.-J., and Yang, X.-Y. (2019c). arXiv:1907.06372 [astro-ph.CO].

Cai, R.-G., Pi, S., and Sasaki, M. (2019d). arXiv:1909.13728 [astro-ph.CO].

Carbone, C., and Matarrese, S. (2005). Phys. Rev. D *71*, 043508. arXiv:astro-ph/0407611 [astro-ph].

Carr, B.J. (1975). The primordial black hole mass spectrum. Astrophys. J. *201*, 1.

Carr, B.J., and Hawking, S.W. (1974). Mon. Not. Roy. Astron. Soc. *168*, 399.

Carr, B., and Kuhnel, F. (2020). Primordial black holes as dark matter: recent developments. Annu. Rev. Nucl. Part. Sci. *70*, 355. arXiv:2006.02838 [astro-ph.CO].

Carr, B.J., Kohri, K., Sendouda, Y., and Yokoyama, J. (2010). Phys. Rev. *D81*, 104019. arXiv:0912.5297 [astro-ph.CO].

Carr, B., Kohri, K., Sendouda, Y., and Yokoyama, J. (2020). arXiv:2002.12778 [astro-ph.CO].

Chang, Z., Wang, S., and Zhu, Q.-H. (2020a). arXiv:2009.11025 [astro-ph.CO].

Chang, Z., Wang, S., and Zhu, Q.-H. (2020b). arXiv:2009.11994 [gr-qc].

Chang, Z., Wang, S., and Zhu, Q.-H. (2020c). arXiv:2010.01487 [gr-qc].

Chen, Z.-C., and Huang, Q.-G. (2018). Merger rate distribution of primordial black hole binaries. Astrophys. J. *864*, 61. arXiv:1801.10327 [astro-ph.CO].

Chen, Z.-C., and Huang, Q.-G. (2019). arXiv:1904.02396 [astro-ph.CO].

Chen, L., Huang, Q.-G., and Wang, K. (2016). Constraint on the abundance of primordial black holes in dark matter from Planck data. J. Cosmol. Astropart. Phys. *1612*, 044. arXiv:1608.02174 [astro-ph.CO].

Chen, Z.-C., Huang, F., and Huang, Q.-G. (2019a). Astrophys. J. *871*, 97. arXiv:1809.10360 [gr-qc].

Chen, Z.-C., Yuan, C., and Huang, Q.-G. (2019b). arXiv:1910.12239 [astro-ph.CO].

Chen, Z.-C., Yuan, C., and Huang, Q.-G. (2021). arXiv:2101.06869 [astro-ph.CO].

Choudhury, S., and Mazumdar, A. (2014). Primordial blackholes and gravitational waves for an inflection-point model of inflation. Phys. Lett. B *733*, 270. arXiv:1307.5119 [astro-ph.CO].

Clesse, S., García-Bellido, J., and Orani, S. (2018). arXiv:1812.11011 [astro-ph.CO].

Cotner, E., Kusenko, A., Sasaki, M., and Takhistov, V. (2019). Analytic description of primordial black hole formation from scalar field fragmentation. J. Cosmol. Astropart. Phys. *2019*, 077. arXiv:1907.10613 [astro-ph.CO].

Dalianis, I. (2020). PoS CORFU2019, p. 096.

Dalianis, I., and Kouvaris, C. (2020). arXiv:2012.09255 [astro-ph.CO].

Dalianis, I., and Kritos, K. (2021). Phys. Rev. D *103*, 023505. arXiv:2007.07915 [astro-ph.CO].

Di, H., and Gong, Y. (2018). J. Cosmol. Astropart. Phys. *07*, 007. arXiv:1707.09578 [astro-ph.CO].

Domènech, G. (2019). arXiv:1912.05583 [gr-qc].

Domènech, G., and Pi, S. (2020). arXiv:2010.03976 [astro-ph.CO].

Domènech, G., and Sasaki, M. (2020). arXiv:2012.14016 [gr-qc].

Domènech, G., Lin, C., and Sasaki, M. (2020a). arXiv:2012.08151 [gr-qc].

Domènech, G., Pi, S., and Sasaki, M. (2020b). J. Cosmol. Astropart. Phys. *08*, 017. arXiv:2005.12314 [gr-qc].

Escrivà, A., Germani, C., and Sheth, R.K. (2020a). Phys. Rev. D *101*, 044022. arXiv:1907.13311 [gr-qc].

Escrivà, A., Germani, C., and Sheth, R.K. (2020b). arXiv:2007.05564 [gr-qc].

Espinosa, J.R., Racco, D., and Riotto, A. (2018). J. Cosmol. Astropart. Phys. *1809*, 012. arXiv:1804.07732 [hep-ph].

Franciolini, G., Kehagias, A., Matarrese, S., and Riotto, A. (2018). J. Cosmol. Astropart. Phys. *03*, 016. arXiv:1801.09415 [astro-ph.CO].

Fu, C., Wu, P., and Yu, H. (2020). Phys. Rev. D *102*, 043527. arXiv:2006.03768 [astro-ph.CO].

Gaggero, D., Bertone, G., Calore, F., Connors, R.M.T., Lovell, M., Markoff, S., and Storm, E. (2017). Phys. Rev. Lett. *118*, 241101. arXiv:1612.00457 [astro-ph.HE].

Gao, Q. (2021). arXiv:2102.07369 [gr-qc].

Gao, T.-J., and Yang, X.-Y. (2019). Gravitational waves induced from string axion model of inflation. Int. J. Mod. Phys. A. *34*, 1950213.

Gao, Q., Gong, Y., and Yi, Z. (2020). arXiv:2012.03856 [gr-qc].

Garcia-Bellido, J., Linde, A.D., and Wands, D. (1996). Phys. Rev. D *54*, 6040. arXiv:astro-ph/9605094 [astro-ph].

Garcia-Bellido, J., Peloso, M., and Unal, C. (2017). J. Cosmol. Astropart. Phys. *09*, 013. arXiv:1707.02441 [astro-ph.CO].

Germani, C., and Musco, I. (2019). Phys. Rev. Lett. *122*, 141302. arXiv:1805.04087 [astro-ph.CO].

Gong, J.-O. (2019). arXiv:1909.12708 [gr-qc].

Graham, P.W., Rajendran, S., and Varela, J. (2015). Phys. Rev. D *92*, 063007. arXiv:1505.04444 [hep-ph].

Green, A.M., and Kavanagh, B.J. (2020). arXiv:2007.10722 [astro-ph.CO].

Griest, K., Cieplak, A.M., and Lehner, M.J. (2013). Phys. Rev. Lett. *111*, 181302.

Hall, A., Gow, A.D., and Byrnes, C.T. (2020). Phys. Rev. D *102*, 123524. arXiv:2008.13704 [astro-ph.CO].

Harada, T., and Jhingan, S. (2016). PTEP, 093E04. arXiv:1512.08639 [gr-qc].

T. Harada, C.-M. Yoo, and K. Kohri, Phys. Rev. D88, 084051 (2013), [Erratum: Phys. Rev.D 89,no.2,029903 (2014)], arXiv:1309.4201 [astro-ph. CO] .

Harada, T., Yoo, C.-M., Nakama, T., and Koga, Y. (2015). Phys. Rev. D 91, 084057. arXiv:1503.03934 [gr-qc].

Hawke, I., and Stewart, J.M. (2002). The dynamics of primordial black-hole formation. Class. Quant. Grav. 19, 3687.

Hertzberg, M.P., and Yamada, M. (2018). Phys. Rev. D 97, 083509. arXiv:1712.09750 [astro-ph. CO].

Hidalgo, J.C. (2007). arXiv:0708.3875 [astro-ph].

Horowitz, B. (2016). arXiv:1612.07264 [astro-ph. CO].

Hütsi, G., Raidal, M., Vaskonen, V., and Veermäe, H. (2020). arXiv:2012.02786 [astro-ph.CO].

Hwang, J.-C., Jeong, D., and Noh, H. (2017). Gauge dependence of gravitational waves generated from scalar perturbations. Astrophys. J. 842, 46. arXiv:1704.03500 [astro-ph.CO].

Inomata, K. (2020). arXiv:2008.12300 [gr-qc].

Inomata, K., and Nakama, T. (2019). Phys. Rev. D 99, 043511. arXiv:1812.00674 [astro-ph.CO].

Inomata, K., and Terada, T. (2019). arXiv:1912. 00785 [gr-qc].

Inomata, K., Kawasaki, M., Mukaida, K., Tada, Y., and Yanagida, T.T. (2017a). Phys. Rev. D 95, 123510. arXiv:1611.06130 [astro-ph.CO].

Inomata, K., Kawasaki, M., Mukaida, K., Tada, Y., and Yanagida, T.T. (2017b). Phys. Rev. D 96, 043504. arXiv:1701.02544 [astro-ph.CO].

Inomata, K., Kawasaki, M., Mukaida, K., and Yanagida, T.T. (2018). Phys. Rev. D 97, 043514. arXiv:1711.06129 [astro-ph.CO].

Inomata, K., Kohri, K., Nakama, T., and Terada, T. (2019a). arXiv:1904.12878 [astro-ph.CO].

Inomata, K., Kohri, K., Nakama, T., and Terada, T. (2019b). Phys. Rev. D100, 043532. arXiv:1904. 12879 [astro-ph.CO].

Inomata, K., Kohri, K., Nakama, T., and Terada, T. (2020a). J. Phys. Conf. Ser. 1468, 012002.

Inomata, K., Kohri, K., Nakama, T., and Terada, T. (2020b). J. Phys. Conf. Ser. 1468, 012001.

Inomata, K., Kawasaki, M., Mukaida, K., Terada, T., and Yanagida, T.T. (2020c). Phys. Rev. D 101, 123533. arXiv:2003.10455 [astro-ph.CO].

Inomata, K., Kawasaki, M., Mukaida, K., and Yanagida, T.T. (2020d). arXiv:2011.01270 [astro-ph.CO].

Ivanov, P. (1998). Nonlinear metric perturbations and production of primordial black holes. Phys. Rev. D 57, 7145. arXiv:astro-ph/9708224 [astro-ph].

Ivanov, P., Naselsky, P., and Novikov, I. (1994). Inflation and primordial black holes as dark matter. Phys. Rev. D 50 (12), 7173.

Jedamzik, K. (1997). Phys. Rev. D 55, 5871. arXiv:astro-ph/9605152.

Jedamzik, K., and Niemeyer, J.C. (1999). Phys. Rev. D 59, 124014. arXiv:astro-ph/9901293.

Kapadia, S.J., Pandey, K.L., Suyama, T., Kandhasamy, S., and Ajith, P. (2020a). arXiv:2009. 05514 [gr-qc].

Kapadia, S.J., Pandey, K.L., Suyama, T., and Ajith, P. (2020b). Phys. Rev. D 101, 123535. arXiv:2005. 05693 [astro-ph.CO].

Kawasaki, M., and Nakatsuka, H. (2019). Phys. Rev. D 99, 123501. arXiv:1903.02994 [astro-ph.CO].

Kawasaki, M., Takayama, T., Yamaguchi, M., and Yokoyama, J. (2006). Phys. Rev. D 74, 043525. arXiv:hep-ph/0605271 [hep-ph].

Kawasaki, M., Kitajima, N., and Yokoyama, S. (2013). Gravitational waves from a curvaton model with blue spectrum. J. Cosmol. Astropart. Phys. 2013, 042. arXiv:1305.4464 [astro-ph.CO].

Kehagias, A., Musco, I., and Riotto, A. (2019). J. Cosmol. Astropart. Phys. 2019, 029. arXiv:1906. 07135 [astro-ph.CO].

Klimai, P.A., and Bugaev, E.V. (2012). In 17th International Seminar on High Energy Physics, 217th International Seminar on High Energy Physics (INR), pp. 163–174. arXiv:1210.3262 [astro-ph.CO].

Kohri, K., and Terada, T. (2018a). Phys. Rev. D97, 123532. arXiv:1804.08577 [gr-qc].

Kohri, K., and Terada, T. (2018b). Primordial black hole dark matter and LIGO/Virgo merger rate from inflation with running spectral indices: formation in the matter- and/or radiation-dominated universe. Class. Quant. Grav. 35, 235017. arXiv:1802.06785 [astro-ph.CO].

Kohri, K., and Terada, T. (2021). Solar-mass primordial black holes explain NANOGrav hint of gravitational waves. Phys. Lett. B 813, 136040. arXiv:2009.11853 [astro-ph.CO].

Kuroda, K., Ni, W.-T., and Pan, W.-P. (2015). Gravitational waves: classification, methods of detection, sensitivities and sources. Int. J. Mod. Phys. D 24, 1530031. arXiv:1511.00231 [gr-qc].

Kuroyanagi, S., Chiba, T., and Takahashi, T. (2018). Probing the Universe through the stochastic gravitational wave background. J. Cosmol. Astropart. Phys. 2018, 038. arXiv:1807. 00786 [astro-ph.CO].

Larson, S.L., Hiscock, W.A., and Hellings, R.W. (2000). Phys. Rev. D 62, 062001. arXiv:gr-qc/ 9909080.

Lin, J., Gao, Q., Gong, Y., Lu, Y., Zhang, C., and Zhang, F. (2020). Phys. Rev. D 101, 103515. arXiv:2001.05909 [gr-qc].

Liu, J., Guo, Z.-K., and Cai, R.-G. (2020). Phys. Rev. D 101, 083535. arXiv:2003.02075 [astro-ph.CO].

Lu, Y., Gong, Y., Yi, Z., and Zhang, F. (2019). J. Cosmol. Astropart. Phys. 12, 031. arXiv:1907. 11896 [gr-qc].

Lu, Y., Ali, A., Gong, Y., Lin, J., and Zhang, F. (2020). arXiv:2006.03450 [gr-qc].

De Luca, V., Franciolini, G., Kehagias, A., and Riotto, A. (2019a). arXiv:1911.09689 [gr-qc].

De Luca, V., Franciolini, G., Kehagias, A., Peloso, M., Riotto, A., and Ünal, C. (2019b). The ineludible non-Gaussianity of the primordial black hole abundance. J. Cosmol. Astropart. Phys. 2019, 048. arXiv:1904.00970 [astro-ph.CO].

De Luca, V., Franciolini, G., Pani, P., and Riotto, A. (2020a). Primordial black holes confront LIGO/ Virgo data: current situation. J. Cosmol. Astropart. Phys. 06, 044. arXiv:2005.05641 [astro-ph.CO].

De Luca, V., Franciolini, G., and Riotto, A. (2020b). On the primordial black hole mass function for broad spectra. Phys. Lett. B 807, 135550. arXiv:2001.04371 [astro-ph.CO].

De Luca, V., Franciolini, G., and Riotto, A. (2021). Phys. Rev. Lett. 126, 041303. arXiv:2009.08268 [astro-ph.CO].

Magee, R., Deutsch, A.-S., McClincy, P., Hanna, C., Horst, C., Meacher, D., Messick, C., Shandera, S., and Wade, M. (2018). Phys. Rev. D98, 103024. arXiv:1808.04772 [astro-ph.IM].

Malik, K.A., and Wands, D. (1998). arXiv:gr-qc/ 9804046 [gr-qc].

Matarrese, S., Pantano, O., and Saez, D. (1993). General-relativistic approach to the nonlinear evolution of collisionless matter. Phys. Rev. D D47, 1311.

Matarrese, S., Pantano, O., and Saez, D. (1994). General relativistic dynamics of irrotational dust: cosmological implications. Phys. Rev. Lett. 72, 320. arXiv:astro-ph/9310036 [astro-ph].

Matarrese, S., Mollerach, S., and Bruni, M. (1998). Phys. Rev. D58, 043504. arXiv:astro-ph/9707278 [astro-ph].

Montero-Camacho, P., Fang, X., Vasquez, G., Silva, M., and Hirata, C.M. (2019). arXiv:1906. 05950 [astro-ph.CO].

Moradinezhad Dizgah, A., Franciolini, G., and Riotto, A. (2019). J. Cosmol. Astropart. Phys. 11, 001. arXiv:1906.08978 [astro-ph.CO].

Musco, I. (2019). Phys. Rev. D 100, 123524. arXiv:1809.02127 [gr-qc].

Musco, I., and Miller, J.C. (2013). Primordial black hole formation in the early universe: critical behaviour and self-similarity. Class. Quant. Grav. 30, 145009. arXiv:1201.2379 [gr-qc].

Musco, I., Miller, J.C., and Rezzolla, L. (2005). Computations of primordial black-hole formation. Class. Quant. Grav. 22, 1405. arXiv:gr-qc/0412063.

Musco, I., Miller, J.C., and Polnarev, A.G. (2009). Primordial black hole formation in the radiative era: investigation of the critical nature of the collapse. Class. Quant. Grav. 26, 235001. arXiv:0811.1452 [gr-qc].

Musco, I., De Luca, V., Franciolini, G., and Riotto, A. (2020). arXiv:2011.03014 [astro-ph.CO].

Nakama, T., and Suyama, T. (2016). Phys. Rev. D *94*, 043507. arXiv:1605.04482 [gr-qc].

Nakama, T., Harada, T., Polnarev, A., and Yokoyama, J. (2014). J. Cosmol. Astropart. Phys. *01*, 037. arXiv:1310.3007 [gr-qc].

Nakama, T., Silk, J., and Kamionkowski, M. (2017). Phys. Rev. D *95*, 043511. arXiv:1612.06264 [astro-ph.CO].

Nakama, T., Suyama, T., Kohri, K., and Hiroshima, N. (2018). Phys. Rev. D *97*, 023539. arXiv:1712.08820 [astro-ph.CO].

Nakamura, K. (2007). Prog. Theor. Phys. *117*, 17. arXiv:gr-qc/0605108 [gr-qc].

Niikura, H., Takada, M., Yasuda, N., Lupton, R.H., Sumi, T., More, S., Kurita, T., Sugiyama, S., More, A., Oguri, M., and Chiba, M. (2019a). Nat. Astron. *3*, 524. arXiv:1701.02151 [astro-ph.CO].

Niikura, H., Takada, M., Yokoyama, S., Sumi, T., and Masaki, S. (2019b). Phys. Rev. D *99*, 083503. arXiv:1901.07120 [astro-ph.CO].

Noh, H., and Hwang, J.-c. (2003). arXiv:astro-ph/0305123 [astro-ph].

Noh, H., and Hwang, J.-c. (2004). Phys. Rev. *D69*, 104011.

Orlofsky, N., Pierce, A., and Wells, J.D. (2017). Phys. Rev. D *95*, 063518. arXiv:1612.05279 [astro-ph.CO].

Özsoy, O., and Tasinato, G. (2020). J. Cosmol. Astropart. Phys. *04*, 048. arXiv:1912.01061 [astro-ph.CO].

Papanikolaou, T., Vennin, V., and Langlois, D. (2020). arXiv:2010.11573 [astro-ph.CO].

Pi, S., and Sasaki, M. (2020). J. Cosmol. Astropart. Phys. *09*, 037. arXiv:2005.12306 [gr-qc].

Pina Avelino, P. (2005). Phys. Rev. D *72*, 124004. arXiv:astro-ph/0510052.

Pitrou, C., Roy, X., and Umeh, O. (2013). xPand : an algorithm for perturbing homogeneous cosmologies. Class. Quan. Grav. *30*, 165002. arXiv:1302.6174 [astro-ph.CO].

Polnarev, A.G., and Musco, I. (2007). Curvature profiles as initial conditions for primordial black hole formation. Class. Quan. Grav. *24*, 1405. arXiv:gr-qc/0605122.

Ragavendra, H.V., Saha, P., Sriramkumar, L., and Silk, J. (2020a). arXiv:2008.12202 [astro-ph.CO].

Ragavendra, H.V., Sriramkumar, L., and Silk, J. (2020b). arXiv:2011.09938 [astro-ph.CO].

Raidal, M., Spethmann, C., Vaskonen, V., and Veermäe, H. (2019). J. Cosmol. Astropart. Phys. *1902*, 018. arXiv:1812.01930 [astro-ph.CO].

Riccardi, F., Taoso, M., and Urbano, A. (2021). arXiv:2102.04084 [astro-ph.CO].

Robson, T., Cornish, N.J., and Liu, C. (2019). The construction and use of LISA sensitivity curves. Class. Quant. Grav. *36*, 105011. arXiv:1803.01944 [astro-ph.HE].

Saga, S., Ichiki, K., and Sugiyama, N. (2015). Phys. Rev. D *91*, 024030. arXiv:1412.1081 [astro-ph.CO].

R. Saito and J. Yokoyama, Phys. Rev. Lett. 102, 161101 (2009), [Erratum: Phys. Rev. Lett. 107, 069901(2011)], arXiv:0812.4339 [astro-ph] .

R. Saito and J. Yokoyama, Prog. Theor. Phys. 123, 867 (2010), [Erratum: Prog. Theor. Phys. 126,351 (2011)], arXiv:0912.5317 [astro-ph.CO] .

M. Sasaki, T. Suyama, T. Tanaka, and S. Yokoyama, Phys. Rev. Lett. 117, 061101 (2016), [erratum: Phys. Rev. Lett. 121,no.5,059901 (2018)], arXiv:1603.08338 [astro-ph.CO] .

Sasaki, M., Suyama, T., Tanaka, T., and Yokoyama, S. (2018). Class. Quant. Grav. *35*, 063001. arXiv:1801.05235 [astro-ph.CO].

Shibata, M., and Sasaki, M. (1999). Phys. Rev. D *60*, 084002. arXiv:gr-qc/9905064.

Siemens, X., Ellis, J., Jenet, F., and Romano, J.D. (2013). The stochastic background: scaling laws and time to detection for pulsar timing arrays. Class. Quant. Grav. *30*, 224015. arXiv:1305.3196 [astro-ph.IM].

Sugiyama, S., Takhistov, V., Vitagliano, E., Kusenko, A., Sasaki, M., and Takada, M. (2021). Testing stochastic gravitational wave signals from primordial black holes with optical telescopes. Phys. Lett. B *814*, 136097. arXiv:2010.02189 [astro-ph.CO].

Thrane, E., and Romano, J.D. (2013). Phys. Rev. *D88*, 124032. arXiv:1310.5300 [astro-ph.IM].

Tisserand, P., Le Guillou, L., Afonso, C., Albert, J.N., Andersen, J., Ansari, R., Aubourg, E., Bareyre, P., Beaulieu, J.P., Charlot, X., et al. (2007). EROS-2). Astron. Astrophys. *469*, 387. arXiv:astro-ph/0607207 [astro-ph].

Tokeshi, K., Inomata, K., and Yokoyama, J.i. (2020). Window function dependence of the novel mass function of primordial black holes. J. Cosmol. Astropart. Phys. *2020*, 038. arXiv:2005.07153 [astro-ph.CO].

Tomikawa, K., and Kobayashi, T. (2019). arXiv:1910.01880 [gr-qc].

Tomita, K. (1967). Non-linear theory of gravitational Instability in the expanding universe. Prog. Theor. Phys. *37*, 831.

Unal, C. (2019). Phys. Rev. D *99*, 041301. arXiv:1811.09151 [astro-ph.CO].

Vaskonen, V., and Veermäe, H. (2021). Phys. Rev. Lett. *126*, 051303. arXiv:2009.07832 [astro-ph.CO].

Wang, S., Wang, Y.-F., Huang, Q.-G., and Li, T.G.F. (2018). Phys. Rev. Lett. *120*, 191102. arXiv:1610.08725 [astro-ph.CO].

Wang, Y.-F., Huang, Q.-G., Li, T.G.F., and Liao, S. (2019a). arXiv:1910.07397 [astro-ph.CO].

Wang, S., Terada, T., and Kohri, K. (2019b). Phys. Rev. *D99*, 103531. arXiv:1903.05924 [astro-ph.CO].

Xu, W.-T., Liu, J., Gao, T.-J., and Guo, Z.-K. (2020). Phys. Rev. D *101*, 023505. arXiv:1907.05213 [astro-ph.CO].

Yi, Z., Gong, Y., Wang, B., and Zhu, Z.-h. (2020a). arXiv:2007.09957 [gr-qc].

Yi, Z., Gao, Q., Gong, Y., and Zhu, Z.-h. (2020b). arXiv:2011.10606 [astro-ph.CO].

Yokoyama, J. (1997). Astron. Astrophys. *318*, 673. arXiv:astro-ph/9509027 [astro-ph].

Yoo, C.-M., Harada, T., Garriga, J., and Kohri, K. (2018). PTEP, 123E01. arXiv:1805.03946 [astro-ph.CO].

Yoo, C.-M., Harada, T., Hirano, S., and Kohri, K. (2021). PTEP *2021*, 013E02. arXiv:2008.02425 [astro-ph.CO].

Young, S. (2019). The primordial black hole formation criterion re-examined: parametrisation, timing and the choice of window function. Int. J. Mod. Phys. D *29*, 2030002. arXiv:1905.01230 [astro-ph.CO].

Young, S., and Byrnes, C.T. (2013). J. Cosmol. Astropart. Phys. *08*, 052. arXiv:1307.4995 [astro-ph.CO].

Young, S., Byrnes, C.T., and Sasaki, M. (2014). Calculating the mass fraction of primordial black holes. J. Cosmol. Astropart. Phys. *2014*, 045. arXiv:1405.7023 [gr-qc].

Young, S., Musco, I., and Byrnes, C.T. (2019). J. Cosmol. Astropart. Phys. *11*, 012. arXiv:1904.00984 [astro-ph.CO].

Yuan, C., and Huang, Q.-G. (2020). arXiv:2007.10686 [astro-ph.CO].

Yuan, C., Chen, Z.-C., and Huang, Q.-G. (2019a). Phys. Rev. *D100*, 081301. arXiv:1906.11549 [astro-ph.CO].

Yuan, C., Chen, Z.-C., and Huang, Q.-G. (2019b). arXiv:1910.09099 [astro-ph.CO].

Yuan, C., Chen, Z.-C., and Huang, Q.-G. (2019c). arXiv:1912.00885 [astro-ph.CO].

Zhang, F., Ali, A., Gong, Y., Lin, J., and Lu, Y. (2020a). arXiv:2008.12961 [gr-qc].

Zhang, F., Gong, Y., Lin, J., Lu, Y., and Yi, Z. (2020b). arXiv:2012.06960 [astro-ph.CO].

Zhou, Z., Jiang, J., Cai, Y.-F., Sasaki, M., and Pi, S. (2020). Phys. Rev. D *102*, 103527. arXiv:2010.03537 [astro-ph.CO].

Zhou, J.-Z., Zhang, X., Zhu, Q.-H., and Chang, Z. (2021). arXiv:2106.01641 [astro-ph.CO].

Zumalacarregui, M., and Seljak, U. (2018). Phys. Rev. Lett. *121*, 141101. arXiv:1712.02240 [astro-ph.CO].